

Synthesis of Zn-Ni-Co Ternary Sulphide Nanoparticles as Electrode Material for Supercapacitors



By

Tanees Nasir

**School of Chemical and Material Engineering
National University of Science and Technology**

2020

Synthesis of Zn-Ni-Co Ternary Sulphide Nanoparticles as Electrode Material for Supercapacitors



Name: Tanees Nasir

Reg. No.: NUST2017NSE05-00000203792

**This thesis is submitted as a partial fulfilment of the requirements for
the degree of**

MS in Nanoscience and Engineering

Supervisor's name: Dr. Muhammad Aftab Akram

School of Chemical and Material Engineering,

National University of Science and Technology,

H-12, Islamabad, Pakistan.

2020



THESIS ACCEPTANCE CERTIFICATE

Certified that final copy of MS thesis written by Ms **Tanees Nasir** (Registration No 00000203792), of School of Chemical & Materials Engineering (SCME) has been vetted by undersigned, found complete in all respects as per NUST Statues/Regulations, is free of plagiarism, errors, and mistakes and is accepted as partial fulfillment for award of MS degree. It is further certified that necessary amendments as pointed out by GEC members of the scholar have also been incorporated in the said thesis.

Signature: _____

Name of Supervisor: **Dr M. Aftab Akram**

Date: _____

Signature (HOD): _____

Date: _____

Signature (Dean/Principal): _____

Date: _____



National University of Sciences & Technology (NUST)

MASTER'S THESIS WORK

Formulation of Guidance and Examination Committee (GEC)

GEC ✓

Name: Tanees Nasir
Department: SCME, NUST
Credit Hour Completed: 24

NUST Regn No: 203792 (NSE-5)
Specialization: MS Nanoscience and Engineering
CGPA: 3.63

Course Work Completed

S/No	Code	Title	Core/Elective	CH	Grade
1	NSE-811	Fundamentals of nanoscience and Engineering	Core	3	A
2	NSE-845	Nanolithography and device fabrication	Elective	3	A
3	MSE-854	Characterization of Materials	Core	3	B+
4	NSE-842	Nanomaterials for energy applications	Elective	3	B+
5	MSE-855	Nanomaterials and nanoprocessing	Core	3	A
6	NSE-821	Nanofabrication by self-assembly	Elective	3	B+
7	NSE-812	Environmental nanotechnology	Elective	3	B+
8	ESE-803	Photovoltaic Devices	Elective	3	B

9 AM-898 Research methodology
Date 04-03-2019

Student's Signature [Signature]

Thesis Committee

- Name: Dr Aftab Akram (Supervisor) Signature: [Signature]
Department: School of Chemicals and Materials engineering
- Name: DR. Mohsin Saleem (Co-supervisor) Signature: [Signature]
Department: School of Chemicals and Materials engineering
- Name: Dr. Zakir Hussain Signature: [Signature]
Department: School of Chemicals and Materials engineering
- Name: Dr. Sofia Javed Signature: [Signature]
Department: School of Chemicals and Materials engineering
- Name: _____ (External) Signature: _____
Department: _____

Date: 8/3/19

Signature of Head of Department: [Signature]

APPROVAL

[Signature]
Date: 8/3/19
Dean/Principal

Date: _____

Distribution

- 1x copy to Exam Branch, Main Office NUST
- 1x copy to PGP Dte, Main Office NUST
- 1x copy to Exam branch, respective institute

School of Chemical and Materials Engineering (SCME) Sector H-12, Islamabad



National University of Sciences & Technology (NUST)

FORM TH-4

MASTER'S THESIS WORK

We hereby recommend that the dissertation prepared under our supervision by
Regn No & Name: 00000203792 Tanees Nasir

Title: Synthesis of Zn-Ni-Co Ternary Sulphide Nanoparticles as Electrode Material for Supercapacitor.

Presented on: 23-Nov-2020 at: 1430 hrs in SCME (on MS Teams)

Be accepted in partial fulfillment of the requirements for the award of Masters of Science degree in Nanoscience & Engineering.

Guidance & Examination Committee Members,

Name: Dr Sofia Javed

Signature: [Signature]

Name: Dr Zakir Hussain

Signature: [Signature]

Name: Dr Mohsin Saleem (Co-Supervisor)

Signature: [Signature]

Supervisor's Name: Dr Muhammad Aftab Akram

Signature: [Signature]

Dated: 23-11-2020

[Signature]

Head of Department

Date 27/11/2020

[Signature]

Dean/Principal

Date 27-11-2020

School of Chemical & Materials Engineering (SCME)

DEDICATION

**I dedicate this thesis to my loving
and caring parents.**

Acknowledgements

All the praises to Almighty Allah, who has given me strength and ability to complete my degree, who is the most beneficent and the most merciful.

I'd like to express my gratefulness to my respected supervisor **Dr. Muhammad Aftab Akram** for his patient guidance that directed me to fulfill my project and this thesis. His humble behavior motivated me to do my best. I am also thankful **Dr. Mohsin Saleem** for taking interest in my research field and for giving expert views and suggestions to make it more productive. Their valuable suggestions and feedback contributed to this thesis. I would also like to thank my parents, family members and friends for their help, prayers, and their valuable suggestions

I also thank **Dr. Sofia Javed** and **Dr. Zakir Hussain** for providing valuable comments, support and guidance through the research. Candid thanks to the staff and management of SCME(NUST) for providing me liberty to enhance my career and establishing this research.

I am extremely thankful to my research fellow Ms Mehreen Shahzadi for providing me the necessary technical suggestions during my research pursuit. Her motivation has been very important in carrying out this research.

I acknowledge the financial aid and technical assistance provided by SCME during my research experience and made this project work possible. Last, but not the least, I want to thank my family for their prayers, support and confidence on me without which I would not have been able to reach my full potential.

-Tanees Nasir

Abstract

Nanostructured zinc-nickel-cobalt sulphide has been established as a promising electrode material due to the synergic enhancement effect of cobalt cations replacement with zinc and nickel. Zinc-nickel-cobalt sulphide (ZNCS) nanoparticles were synthesized using a facile hydrothermal route followed by annealing treatment. For a comparative study, nanostructures of nickel cobalt sulphide (NCS) and nickel sulphide (NS) were also synthesized via same method. The synthesized samples were characterized through versatile techniques such as XDR; for structural analysis, SEM for morphological analysis; and for electrochemical studies, CV and GCD tests were run. These tests affirmed the developed ZNCS nanoparticles for supercapacitors. ZNCS nanoparticles exhibit specific capacitance of $2113.173 \text{ F g}^{-1}$ at 5 Ag^{-1} . Cyclic stability test conducted revealed that ZNCS possesses good electrochemical performance; 99.4 % specific capacitance was retained for up to 1000 charge-discharge cycles.

Table of Contents

Chapter 1 Introduction:	1
1.1 Historical background:	1
1.2 Renewable energy sources:	3
1.3 Energy storage devices:	4
1.3.1 Fuel cells.....	5
1.3.2 Batteries:.....	6
1.3.2.1 Primary batteries:	7
1.3.2.2 Secondary batteries:	7
1.3.3 Capacitors:	8
1.3.4 Super capacitors:	9
1.3.4.1 Electric Double Layer Capacitors (EDLC):	10
1.3.4.2 Pseudo-capacitors:.....	12
1.3.4.3 Hybrid capacitors:	13
1.4 Comparison between batteries and supercapacitors:.....	14
1.5 Electrode materials for supercapacitors:	15
1.5.1 Carbon materials:	16
1.5.1.1 Activated carbon:	17
1.5.1.2 Carbon nanotubes:.....	18
1.5.1.3 Graphene:	18
1.5.2 Polymers:.....	19
1.5.2.1 Polyaniline:.....	20

1.5.2.2 Polypyrrole:	22
1.5.3 Metal oxides:	23
1.5.4 Metal sulphides:	24
Chapter 2 Experimental methods.....	27
2.1 Synthesis routes:	27
2.2 Top-down synthesis route:	27
2.3 Bottom-up synthesis route:.....	28
2.3.1 Sol-gel method:	29

2.3.2 Hydrothermal/solvothermal synthesis route:.....	31
2.3.3 Co-precipitation synthesis route:	32
2.3.4 Microwave-assisted synthesis:	33
2.3.5 Micro-emulsion synthesis route:	35
2.3.6 Sonochemical synthesis:.....	36
2.4 Aims and objectives:	37
Chapter 3 Literature review	39
Chapter 4 Material synthesis:	47
4.1 Apparatus required:	47
4.2 Synthesis of Nickel Sulphide:	47
4.3 Synthesis of Nickel Cobalt Sulphide (NCS):	49
4.4 Zinc Nickel Cobalt Sulphide (ZNCS) synthesis:	51
Chapter 5 Characterization techniques	54
5.1 Scanning Electron Microscopy:	54
5.2 XRD:	56
5.3 Field emission scanning electron microscope (FESEM):	59
5.3.1 Source of electrons:	60
5.3.2 Segment with lenses and apertures:.....	61
5.3.3 Condenser lens:	61
5.3.4 Scan coils:.....	61
5.3.5 Objective lens:	61
5.3.6 Stigmator coils:.....	62
5.3.7 Image formation:	62
5.4 Electron dispersive spectroscopy (EDX):	62
5.5 Electrochemical Analysis:.....	65

5.6 Cyclic Voltammetry:	68
5.7 Galvanostatic Charge-Discharge (GCD):	69
5.8 Cyclic stability:	71
Chapter 6 Results and discussion	72
6.1 X-ray diffraction (XRD):	72
6.2 Field emission scanning electron microscope (FESEM):	73
6.3 Electron dispersive spectroscopy (EDX):	77
6.6 Cyclic Voltammetry (CV):	81
6.6.1 Nickle Sulphide:	82
6.6.2 Nickel Cobalt Sulphide:	83
6.6.3 Zinc Nickel Cobalt Sulphide:	84
6.7 Galvanostatic charge-discharge (GCD):	85
6.7.1 Nickle Sulphide:	85
6.7.2 Nickle Cobalt Sulphide:	86
6.7.3 Zinc Nickle Cobalt Sulphide:	87
6.8 Cyclic stability:	88
Conclusion.....	90
References	91

List of tables:

Table 1.1 Types of energy sources:.....	3
Table 1.2 Classification of supercapacitors:	10
Table 1.3 Comparison between batteries and supercapacitors:	14
Table 1.4 Comparison between capacitors, batteries and supercapacitors:	15
Table 1.5 Classification of supercapacitor electrode materials:.....	15
Table 4.1 Apparatus used for the synthesis process:.....	48
Table 4.2 Materials used for the synthesis of nickel sulphide:	47
Table 4.3 Materials used for the synthesis of nickel cobalt sulphide:	50
Table 4.4 Materials used for the synthesis of zinc nickel cobalt sulphide:.....	52
Table 6.1 EDS of elements analysis of ZNCS:.....	78
Table 6.2 EDS of elements analysis of NCS:	80
Table 6.3 EDS of elements analysis of NS:	81

List of Figures:

Figure 1-1: Ragone plot	2
Figure 1-2: Schematic representation of a fuel cell	5
Figure 1-3: Schematic representation of a battery	7
Figure 1-4: schematic representation of a conventional capacitor.....	8
Figure 1-5: schematic representation of a supercapacitor.....	9
Figure 1-6: schematic representation of an EDLC.....	11
Figure 1-7: schematic representation of pseudo-capacitors	13
Figure 1-8: schematic representation of hybrid capacitors	14
Figure 2-1: schematic representation of sol-gel synthesis	30
Figure 2-2: schematic representation of hydrothermal synthesis.....	31
Figure 2-3: schematic representation of co-precipitation route	32
Figure 2-4: schematic representation of microwave-assisted synthesis route	34
Figure 2-5: schematic representation of micro-emulsion synthesis route.....	35
Figure 2-6: schematic representation of sonochemical synthesis route	36
Figure 3-1: Number of research publication on supercapacitors from the year 2000-2010	39
Figure 3-2: Publications on electrode materials.....	39
Figure 4-1: Nickel Sulphide synthesis process flow	49
Figure 4-2 Nickel Sulphide synthesis process flow	51
Figure 4-3: Zinc Nickel Cobalt Sulphide synthesis process flow	53
Figure 5-1: Scanning Electron Microscope (SEM) system	54
Figure 5-2: schematic representation of a scanning electron microscope instrument	55
Figure 5-3: X-Ray Diffraction (XRD) system	57

Figure 5-4: Schematic arrangement of XRD Diffractometer components	58
Figure 5-5: Schematic representation of x-ray emission.....	64
Figure 5-6: Schematic representation of an Electrochemical workstation electrode assembly	66
Figure 5-7: Cyclic voltammogram curves of (a) ideal capacitor, (b) EDLC, and (c) pseudocapacitive materials.....	69
Figure 5-8: GCD curves of (a) EDLC (b)Pseudo capacitor	70
Figure 6-1: XRD spectrum of NS, NCS and ZNCS	73
Figure 6-2: XRD spectrum of NS, NCS and ZNCS	74
Figure 6-3: FESEM analysis of Zinc Nickle Cobalt Sulphide.....	75
Figure 6-4: FESEM analysis of Nickle cobalt sulphide.....	76
Figure 6-5: FESEM analysis of Nickle sulphide.....	77
Figure 6-6: EDS spectrum of NCS	78
Figure 6-7: EDS spectrum of ZNCS	79
Figure 6-8: EDS spectrum of NS	80
Figure 6-9: CV of Nickle Sulphide (NS)	83
Figure 6-10: CV of Nickel Cobalt Sulphide (NCS).....	84
Figure 6-11: CV of Zinc Nickel Cobalt Sulphide (ZNCS).....	85
Figure 6-12: GCD of Nickle Sulphide (NS)	86
Figure 6-13: GCD of Nickle Cobalt Sulphide (NCS).....	87
Figure 6-14: GCD of Zinc Nickle Cobalt Sulphide (ZNCS)	88
Figure 6-15: Cyclic stability of Zinc Nickle Cobalt Sulphide (ZNCS)	89

Chapter 1

1.Introduction:

The ever-growing, amplified demand for energy has us exploiting our plants resources such as fossil fuels, natural gas, radioactive materials etc. All such sources are quantifiably limited and this spurs on an interest to look toward availing the benefits of renewable energy sources such as tidal power, solar power, wind power, etc. This, of course is limited by the low efficiency from such ‘green’ sources. Currently, more than half of the world’s energy demands are met by utilizing the far more environmentally damaging fossil fuel sources, by burning coal, exploiting the riches of natural gas and nuclear materials. These riches are depleting at an alarming pace and in result to their usage are already wreaking havoc on our planet’s environment. Utilization of such non-renewable sources results in smoke invariably being released into the atmosphere. This toxic release contains harmful gases such as carbon dioxide, sulphur dioxide, zinc, etc. These fatal emissions have been causing cataclysmic effects not only to humans and animals, but are also polluting the water we drink, the crops we grow, the air we breathe; ensuing devastating health issues and catastrophic environmental damage[1]. Such disastrous impacts spur us on to seek and explore not only environmentally friendly energy sources, but to also pursue research for new and improved materials and devices that can meet our energy demands, leave a small carbon footprint, are cost effective and can be utilized over a wide range of applications[2].

One such device is a supercapacitor or ultracapacitor [3]. These devices have gained the spotlight due to their fast charging-discharging phenomenon, simple mode of operation, longer life cycles (greater than 100,000 cycles), high power density in comparison with batteries and a high energy density in comparison with conventional capacitor [4].

1.1 Historical background:

Electrochemical capacitors or ultracapacitors, more notably recognized as supercapacitors are energy storage devices discovered in late 1950s. During 1950s and

1970s, the first experiments were conducted by Standard Oil of OHIO (SOHIO) and General Electric (GE) that resulted in the fabrication of supercapacitors comprising of electrodes made up of carbon materials constituting a high surface area. These initial experiments produced a device whose capacitance was calculated to be $\sim 1\text{F}$. In early 1980s, RuO_2 electrodes were employed that enhanced the electrochemical activity in the supercapacitor and had a low equivalent series resistance (ESR). This resulted in a calculation of capacitance $\sim 1\text{kF}$ of that device[6].

One of the major advantages electrochemical capacitors offer is their ability to bridge the gap between batteries and conventional capacitors. Supercapacitors are advantageous to use where we need to release a colossal amount of power (discharging) in a very short time. These devices store a higher amount of energy than capacitors and charge quickly, thus opening a very broad revenue of usage[7, 8]. A lot of research is being carried out towards developing better electrochemical capacitors with longer lasting life, larger gravimetric and volumetric energy storage, shorter charging/discharging times and cost effectiveness[9, 10].

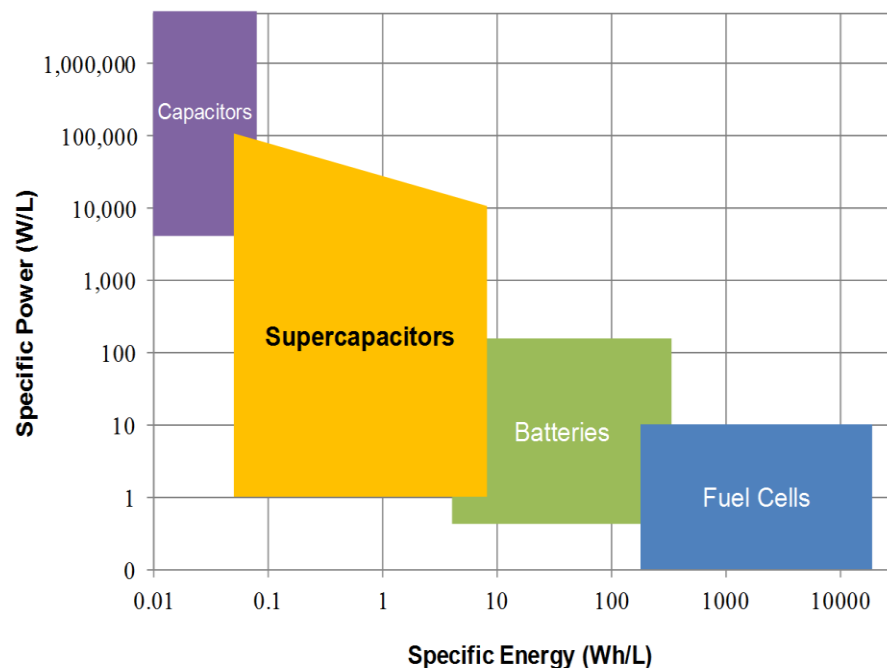


Fig. 1.1: Ragone plot

From the Ragone plot in fig 1.1, we gather a comparison between energy storage performances of different energy storage devices. This plot comprises of specific power (W/kg) and specific energy (Wh/kg) on both of its logarithmically aligned axes[11].

$$\text{specific energy} = \frac{V \times I \times t}{m}$$

Specific power can be defined as power delivered per unit mass and specific energy defines how quickly energy is delivered to an externally applied load[12].

$$\text{specific power} = \frac{V \times I}{m}$$

1.2 Renewable energy sources:

As the name suggests, renewable energy sources offer the capability to be reused. In comparison with renewable technology, non-renewable energy sources produce toxic waste at a colossal scale, damage the environment, cause pollution of all kinds, notoriously contribute to greenhouse gas effect and also pose a very serious threat to health of humans and animals[13].

There are two vital categories of energy sources:

Table 1.1: types of energy sources

Energy Sources	
Power plants	Renewable energy sources
Nuclear power stations	Wind energy
Fossil fuels	Solar energy
Incineration plants	Hydrothermal energy
Coal thermal power plant	Geothermal power
Natural gas	Bio-mass

Renewable energy sources comprise of wind, sunlight, geothermal heat, tidal energy, biomass and hydroelectric power and are consumed at our expediency as these

do not pose a threat to our environment nor they can be depleted with time[14, 15]. These environmentally friendly sources produce a very minute amount of waste that can be easily taken care of. Such energy sources are also referred to as 'green energy'. Renewable energy sources are cost-effective, make up for more than 10% of our electrical usage and are quickly replenished at a very fast pace after consumption.

Theoretically, renewable energy sources should fill in for 100% of the world energy consumption, but realistically, that is not probable. Their major disadvantage arises since these sources are less efficient than non-renewable energy sources[16].

1.3 Energy storage devices:

By definition, an energy storage device is a system that is used to store in and extract energy from when desired. With the growing concern to tackle the current worsening global warming issue, the use of renewable energy sources and efficient energy storage devices play a vital role in our lives[17]. Renewable energy sources produce a varying power generation and thus, we need advanced energy systems to store that power to be utilized at any desired time. Currently, a race is going on to develop better and more efficient energy storage devices that can be utilized efficiently, effectively and for longer periods of time, even in remote areas away from a transmission grid. In addition to this, smaller and smaller energy storage devices are being manufactured. Some of which are as small as a tiny button; they store and deliver megawatts per hour of energy effectively[18, 19].

Presently, energy storage systems are classified into the following:

- Mechanical
- Chemical
- Electrical
- Electrochemical

And state-of-the-art energy storage devices are classified into the following categories:

- Fuel cells
- Batteries

- Supercapacitors
- Capacitors

1.3.1 Fuel cells

Fuel cells are electrochemical systems that much like a battery, convert chemical energy into electrical energy. But unlike a battery, these devices do not need to be recharged. As long as there is a steady fuel supply present, these electrochemical cells will run.

As visible in fig. 1.2, an electrolyte is sandwiched between two oppositely charged electrodes. This electrolyte possesses high ion conductivity and high electron resistivity. Fuel cell operates when a fuel such as hydrogen is supplied through channels in the anode. The catalyst (usually a carbon cloth with platinum nanoparticles embedded onto its surface) splits the hydrogen molecules into hydrogen ions and electrons. The anode conducts the electrons to an externally applied load while hydrogen ions travel through the ion conductive electrolyte to the cathode. At the cathode, oxygen is being supplied which oxidizes the incoming hydrogen atoms reuniting with electrons coming in through the external load. The products of such a fuel cell are heat, electricity and water[20].

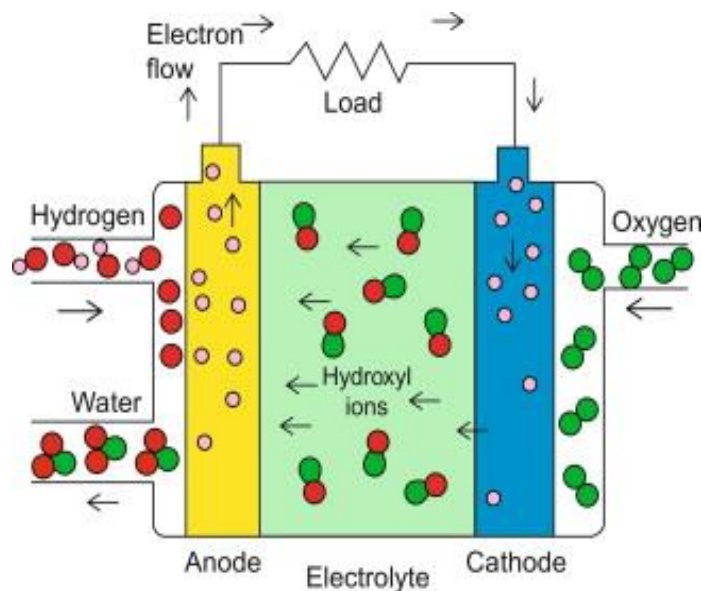


Fig. 1.2: schematic representation of a fuel cell

Due to a lack of toxic and harmful by-products, this technology is safer and greener in comparison with combusting fossil fuels, burning coal or nuclear grids. This amazing green technology has potential applications ranging from running a power grid station to powering a laptop. Their drawback lies with the expensive technology required to produce and store hydrogen fuel. Thus, research is being carried on different electrode materials, electrolytes and fuels in order to commercialize this technology at a reasonable consumer cost[21].

Currently, these environmental-friendly electrochemical devices are being employed in hydrogen powered vehicles, space shuttles, portable electronic devices, military systems, etc. Small sized fuel cells can be used in cell phones as well, but this technology is expensive in terms of a large-scale production[22].

1.3.2 Batteries:

A battery is an electrochemical device that converts chemical energy into electrical energy upon the connection of an external load.

As observable by the following schematic, battery components comprise of an anode (+), a cathode (-), an electrolyte and a separator (advanced technology). Redox reactions take place inside a single or multiple electrochemical cells when an external load is applied. Multiple cells are connected in a series fashion. When an externally attached load is connected to the battery terminals, electrons flow across the load between the battery current collectors while the ions travel through the electrolyte present. This flow of electrons powers the load e.g. a light bulb, laptop, mobile phones, etc.

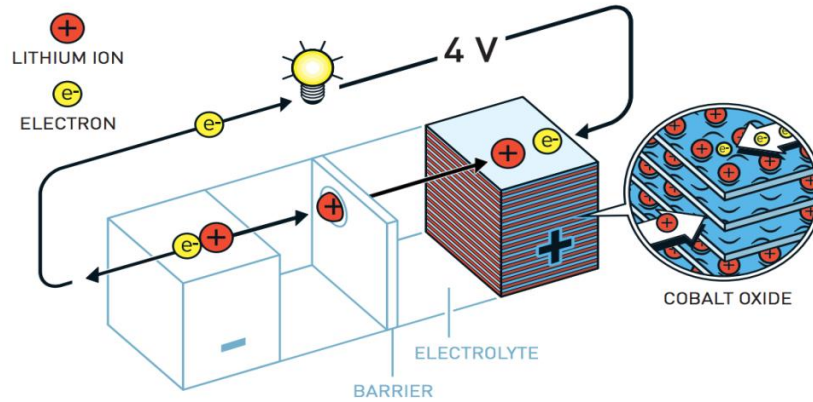


Fig. 1.3: schematic representation of a battery

There are two types of batteries:

1.3.2.1 Primary batteries:

In primary batteries, the electrochemical reactions are irreversible and thus, once consumed, these batteries cannot be recharged and are tossed away after a single use. These cells have high specific energy and low power consumption which aids these batteries to last longer. Zinc dry cells are an example of primary batteries.

These tiny portable devices can only be used in devices with a lower current consumption e.g. wrist watches, flash lights, pacemakers, remote controls.

1.3.2.2 Secondary batteries:

Also known as a rechargeable battery type, in secondary batteries, electrochemical reactions can be reversed by applying a particular value of voltage in the opposite direction (to charging). This battery type is suitable of applications where high current consumption is a vital requirement. Lead-acid, Nickel-Cadmium, Lithium-ion, sodium-ion, potassium-ion batteries are some examples of this type.

Depending upon the chemistry of a secondary battery; the choice of electrodes, electrolyte and separator, different battery types are garnered over the years. This chemistry is vital as the chemistry holds dominion over the energy density, power density, life-cycle, charging/discharging time, cost and efficiency of a battery[23].

Secondary batteries have four major categories:

- Lead-acid
- Nickel-Cadmium
- Lithium-ion
- Nickel-metal Hydride

Secondary batteries are used in mobile phones, quad-copters, vehicles, appliances, inverters, etc. Batteries can be aqueous or non-aqueous.

1.3.3 Capacitors:

In a conventional capacitor, two conducting plates are placed facing each other in a parallel fashion, separated at a small distance by a dielectric e.g. air. When potential is applied across these plates, an electric field generates between them and charges accumulate on the surface of the two charged plates as represented in fig. 1.4:

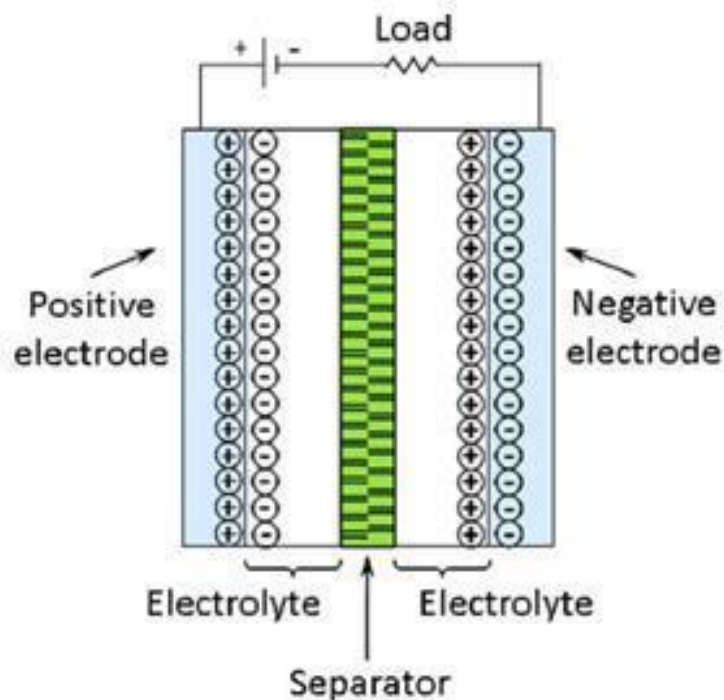


Fig. 1.4: schematic representation of a conventional capacitor

However, conventional capacitors store a diminutive amount of energy; associated with geometric constraints and limited surface area for charge storage[25].

They store energy electrostatically, thus, resulting in them having a small energy density. These devices are known for their higher power densities and long cycle life. Capacitance (C) is defined by charge (Q) accumulated on the plates of a capacitor under the influence of an applied external voltage (V);

$$C = \frac{Q}{V}$$

For conventional capacitors, capacitance ranges from micro (μ) to pico (p) farads (F). Capacitance of a parallel plate capacitor is dependent upon the following factors:

$$C = \epsilon \frac{A}{d}$$

Where, ‘C’ represents capacitance of the device, ‘A’ represents surface area of the electrode plates, ‘d’ represents the parting distance between the two plates present and constant ‘ ϵ ’ represents permittivity of free space (i.e. properties of the dielectric medium), whose value is 8.85×10^{-12} F/m.

1.3.4 Supercapacitors:

Supercapacitors have gained interest as these cells possess long cyclic-life and bridge the gap between two types of energy storage systems i.e. batteries and capacitors. These electrochemical gadgets manifest energy density that of batteries whilst also incorporating the power density that of capacitors[26].

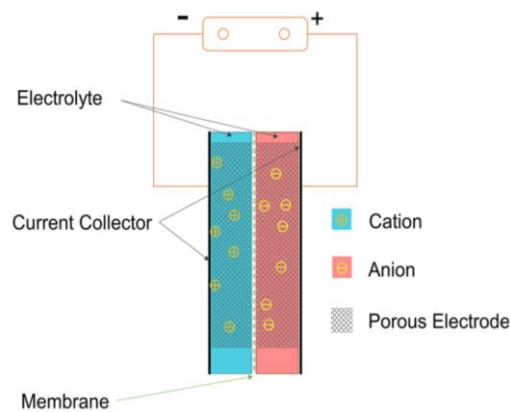


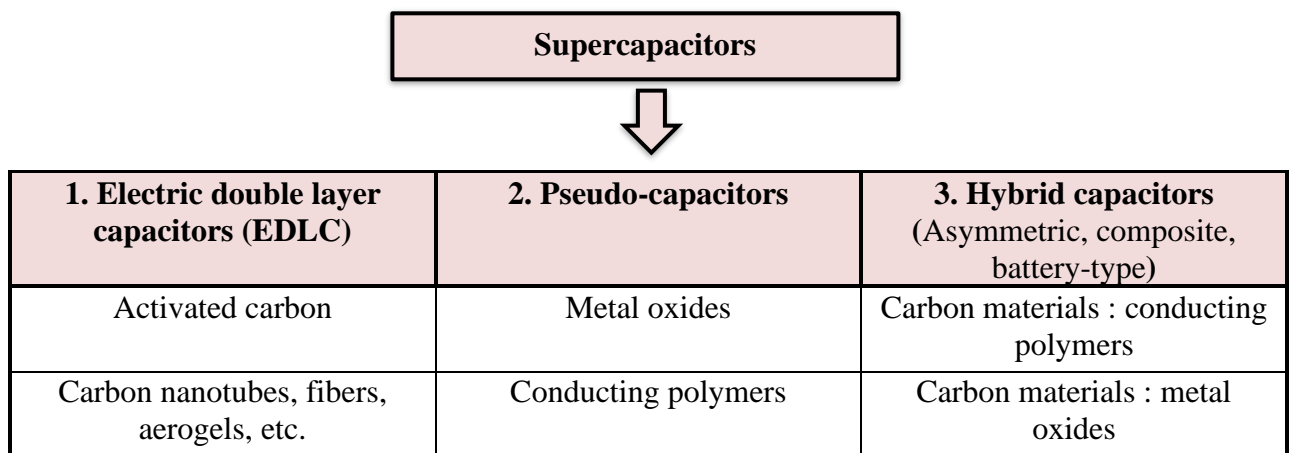
Fig. 1.5: schematic representation of a supercapacitor

Supercapacitors, also termed as electrochemical capacitors or ultra-capacitors, are energy storage gadgets; where, there are two oppositely charged electrodes immersed in a present electrolyte. The electrodes constitute of high surface area materials such as porous carbonaceous material or a variation of metal oxides. During operation, charges amass on the electrode-electrolyte interface. The current collectors are separated, at a minute distance (few nanometers), by an ion-permeable separator in order to avoid any short-circuiting in the device. This assembly is immersed in an electrolyte that serves the function of an ion reservoir. Electrolyte can be ionic liquids, aqueous or organic solutions.

The operating voltage of this electrochemical cell largely depends upon the choice of the electrolyte present i.e. the decomposition voltage of electrolyte (for aqueous electrolytes, it is $\sim 1.2V$). The decomposition voltage influences the energy density of the device.

Supercapacitors are further classified into the following three types; each with its unique properties:

Table 1.2: classification of supercapacitors



1.3.4.1 Electric Double Layer Capacitors (EDLC):

The charge storage mechanism in an electric double layer capacitor is similar to that of a conventional capacitor. EDLCs are the type of supercapacitors where, ideally

speaking, charge is stored electrostatically and no faradic; reduction-oxidation, reactions are involved. The electrostatic charge storage is reversible and thus, ensures an increased life-cycle of the device.

Electrostatic charge storage takes place on the electrode-electrolyte interface. When an external potential is applied, an electric field develops between the oppositely charged electrodes. On a cathode surface, electrons accumulate and thus, these surface electrons attract the positively charged ions from the electrolyte. The oppositely charged electrolyte ions adsorb on the surface thus, neutralizing the unabridged charge of the electrode. The ions are separated from the electrode by a mono-molecular distance. This polarized solvent molecular layer is referred to as the Inner Helmholtz Layer (IHL) and the adsorbed electrolyte-ion layer is referred as the Outer Helmholtz Layer (OHL). The OHL is compact and attracts the oppositely charges ions from the electrolyte; now, this layer is referred to as the Diffused sheet as the charged ions are loosely bound to the double layer, in a disordered fashion, as shown in fig.1.6:

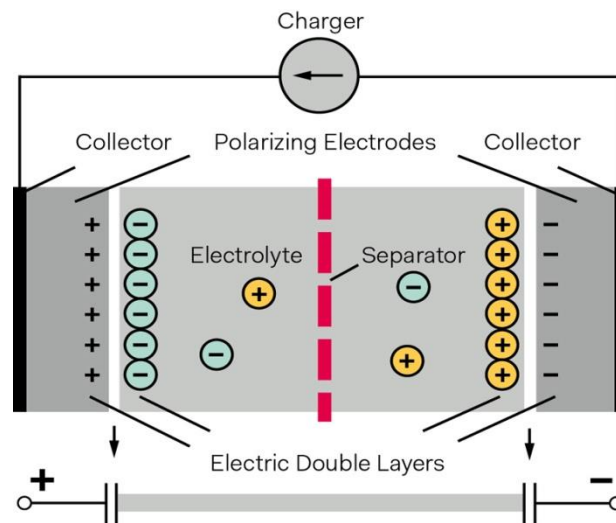


Fig. 1.6: schematic representation of an EDLC

Thus, no charge transfer or ion exchange occurs between the present electrode and electrolyte. In case the electrode surface is porous with pore size less than 1nm, the electrolyte ions can easily penetrate these pores and get adsorbed on the electrode surface, therefore, resulting in an increased capacitance. Due to an enhanced interfacial

area and atomic distance separation of opposite charges, EDLCs have way larger capacitances as compared to conventional capacitors[27].

1.3.4.2 Pseudo-capacitors:

In addition to electrostatic storage, supercapacitors can also store charge electrochemically that contribute to the increase in the energy density of supercapacitors. This type of supercapacitors is known as a pseudo-capacitor. In pseudo-capacitors fast Faradic reactions take place with fast reversibility. In comparison with batteries, fewer reaction products result in a pseudo-capacitor; which enhances the life-cycle of the electrochemical device and contributes to the energy density as well[28]. Charge transfer takes place due to intercalation, electrosorption and redox reactions occurring between the electroactive materials i.e. electrode and electrolyte.

Pseudo-capacitors possess higher power density than batteries but a lower power density than EDLCs. Unlike the redox reactions that occur in a battery, pseudo-capacitors have faradic reactions, resulting in the accumulation of charges on the electrode, which are subject to a thermodynamic change of potential. This gives rise to better reversibility and higher power density. These electrochemical devices have energy density that is inferior than that of a battery and higher in comparison with EDLCs. Pseudo-capacitors have energy density 10-100 times higher than that of EDLCs.

Due to reversible redox reactions taking place between the electroactive materials, phase changes occur in the device, therefore, reducing the life-cycle. Since EDLCs store charge electrostatically, physical changes occur in the device, thus, their life-cycle is longer than Pseudo-capacitors[29]. Since, intercalation of charges ensues at the interface between the electrode material and the electrolyte in attendance, the morphology of the material is as predominantly indispensable as is the case in EDLCs.

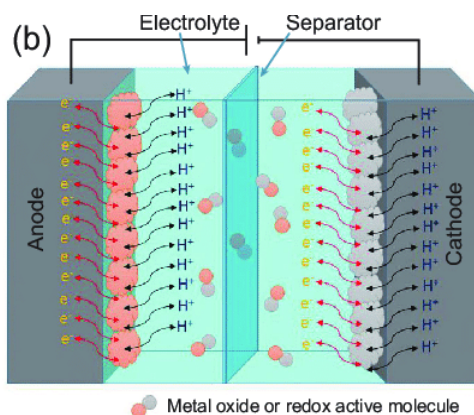


Fig. 1.7: schematic representation of pseudo-capacitors

Electrodes comprise of polymeric materials or oxides such as RuO_2 , NiCo_2O_4 , etc. Carbon based materials such as CNTs can also be used. As carbon based materials exhibit good capacitance but low faradic yield, such materials can have their surface functionalized with oxygen containing functional groups. Research based studies have revealed that oxygen-functionalized carbonaceous material electrodes exhibit a ~5% increase in their Faradic behavior while simultaneously enhancing ~30% capacitance of the carbon electrode.

1.3.4.3 Hybrid capacitors:

This type involves the combination of pseudo-capacitor and EDLC materials. The assembly of electrodes comprises an asymmetric fashion; due to the presence of one electrode (CNTs, rGO, GNPs, etc.) exhibiting EDLC behavior for charge separation and the other electrode (PbO_2 , MnO_2) exhibiting pseudo-capacitative behavior. This results in different electrode materials; working at different operating potential windows, complementing the overall potential window of the device. Hybrid capacitors are also referred to as ‘capatteries’; an amalgamation of the words: ‘capacitor’ and ‘battery’.

We observe that since the electrode comprises of a composite material (e.g. RuO_2/CNTs), the localized redox active sites are very close to one another with a large difference in energy states. Thus, a delocalized electron travels back and forth from these redox active sites over a wide potential window[30].

This type displays high energy density, good cyclic stability, excellent specific capacitance and power density than the previous two types.

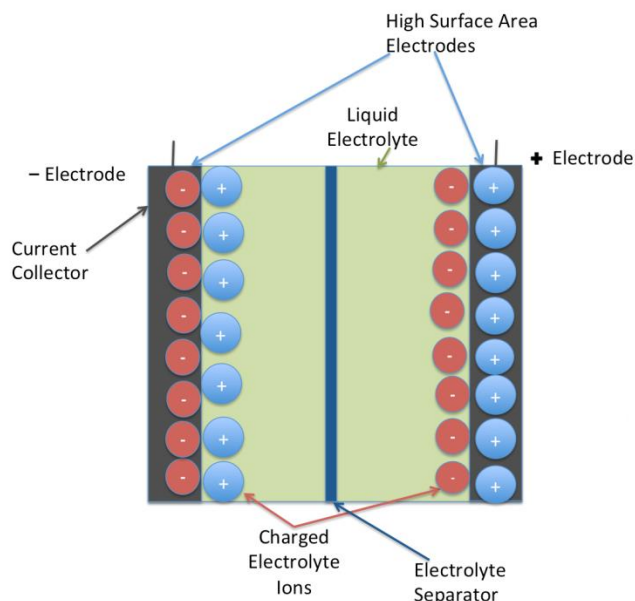


Fig. 1.8: schematic representation of hybrid capacitors

1.4 Comparison between batteries and supercapacitors:

Batteries and supercapacitors are two electrochemical systems with a lot of similarities as well as differences. Their course of function is what is considered for their use in potential applications. Table 1.7 discusses some crucial parameters between these two energy storage devices.

Table 1.3: comparison between batteries and supercapacitors

Comparison parameter	Battery	Supercapacitor
Storage mechanism	Chemical	Physical
Power limitation	Reaction kinetics, mass transport	Electrolyte conductivity
Energy storage	High (bulk)	Limited (surface area)
Charge rate	Kinetically limited	High, same as discharge
Cycle life limitations	Mechanical stability, chemical reversibility	Side reactions

Table 1.4: comparison between capacitors, supercapacitors and batteries

Characteristics	Capacitor	Supercapacitor	Battery
Specific energy (Wh/kg)	< 0.1	1 to 10	10 to 100
Specific power (W/kg)	> 10,000	500 to 10,000	< 1000
Discharge time	10^{-6} to 10^{-3}	Seconds to minutes	0.3 to 3 hours
Charge time	10^{-6} to 10^{-3}	Seconds to minutes	1 to 5 hours
Coulombic efficiency	About 100 %	85 % to 98 %	70 % to 85 %
Cycle life	Almost infinite	> 500,000	~ 1000

1.5 Electrode materials for supercapacitors:

Capacitance is elucidated as the amount of charge separated due to a field gradient that forms under the influence of an applied voltage. In a capacitor, the charge separation results in an accumulation of charges on the interface between the electrode and electrolyte present. The more amount of charge is separated, the higher the capacitance of a material[31]. Similarly, the performance of a supercapacitor is largely based on its ability to separate and accumulate a large amount of charge i.e. an enhanced capacitative behaviour of the electrode.

Electrode materials are categorized into the following three vital categories:

Table 1.5: classification of supercapacitors electrode materials

Supercapacitor electrode materials		
Polymers	Carbon materials	Oxides
Polyaniline	CNTs, rGO, etc.	PbO ₂ , RuO ₂
Polypyrrole, etc.	Activated carbon	MnO ₂ , etc.

In supercapacitors, we employ nanostructured materials owning a high degree of porosity, large pore volume and a high specific surface area. Employing porous materials has an advantage of having a high surface area i.e. more active redox reaction

sites are available which result in an increase in the capacitance of the electrochemical device.

1.5.1 Carbon materials:

Due to their abundant availability, inexpensive, low toxicity, high electrical conductivity easy processing, mass production availability, good chemical and electrochemical stability, easy to engineer and incorporate into different structures and high specific capacitance, carbonaceous materials are one of the considerably appreciable materials mostly employed in the manufacturing of supercapacitors.

The CV curve of carbonaceous materials appears somewhat rectangular due to surface charge accumulation and GCD reveals linear curve.

Commercially, a lot of supercapacitors have employed porous carbonaceous materials namely activated carbon in the fabrication of supercapacitor electrodes[32]. Carbon-based materials represent a wide assortment of different carbon structures that have been profoundly and amply studied as components for supercapacitors; such as:

- Carbon nanotubes (one dimensional)
- Graphene sheets (two dimensional)
- Carbon dots (zero dimensional)
- Porous activated carbon
- Carbon nanofibers
- Carbon aerogels
- Mesoporous carbon foams (three dimensional).

Carbonaceous materials showcase their energy storage mechanism by storing electrical charge in an electric double layer charge (EDLC) storage operation. Electrical charge is stored at the interface between the active material deposited onto the electrode

and the electrolyte present rather than in the bulk of the active matter; which is why the excessive surface area availability for the accumulation of charge is crucial. The high-surface area availability enhances specific capacitance and energy density of the respective supercapacitor gadget. An increase in porosity is one pivotal way of augmenting the specific capacitance. The size of ions and pores must be optimal for the sieving effect. Micropores ($2\text{nm} < d < 50\text{nm}$) contribute to an increased capacitance as compared to mesopores ($d > 50\text{nm}$). This is due to enhanced electroadsorption of electric double layer (EDLC) made possible due to the more porous surface area availability in micropores than that in mesopores[33]. Mesopores on the surface are equally important to transport ions from the electrolyte present to the micropores of the active material.

The specific surface area of carbonaceous materials can also be increased by activation of the respective material surface; by functionalizing their surface. Functionalization of heteroatoms, prompt the wettability of the surface of active material which in turn, enhance faradic redox reaction sites. Induction of surface functional groups such as sulphur, oxygen, nitrogen and boron have been extensively investigated on carbonaceous materials that have evinced high specific capacitance. Carbonaceous materials evince high rate performance which can be attributed to their swift electrical charge transport due to low electrical resistance.

It has been reported that excessive surface activation can result in a colossal pore volume which, in turn, lead to low conductivity and a decrease in material density. This results in power capability loss as well as low volumetric energy density.

1.5.1.1 Activated carbon:

One of the most frequently employed genus of carbon as an active material for supercapacitor electrodes is activated carbon (AC).

In comparison with graphene and carbon nanotubes (CNTs), activated carbon is cheaper in cost and shows significantly high surface area. Activated carbon materials are extracted from raw sources such as saw-dust, wood by-products, nutshells, brown coal, black coal and petroleum coke. The precursors undergo carbonization via thermal or

chemical activation. The activation process results in activated carbon with a high surface area[34].

1.5.1.2 Carbon nanotubes:

Carbon nanotubes evince high conductivities, good porous structure, good mechanical strength, ballistic electron transport (no back-scattering of electrons as it gives rise to electrical resistance), excellent chemical properties, etc. Supercapacitor electrodes that employ high surface area CNTs as active materials exhibit almost the same capacitance as activated carbon electrodes.

Carbon nanotubes can be extracted simply from the decomposition of hydrocarbons. Depending upon the parameters of the employed synthesis process, multi-walled carbon nanotubes (MWCNTs) or single-walled carbon nanotubes (SWCNTs) can be obtained. They can be functionalized to achieve higher capacitances.

As with activated carbon, carbon nanotubes are also chemically or physically activated to increase their surface area. Surface activation results in the appearance of micropores on the surface of CNTs which results in better capacitative performance[35]. CNTs are also paired with other materials (polymers, oxides, sulphides) as composites as supercapacitors electrodes.

1.5.1.3 Graphene:

Following its discovery in 2004, graphene has been colossally researched on due to its tremendous properties which are required for high-performance energy systems. Graphene possesses zero band gap which results in high conductivity. It also possesses short diffusion length for electron transport. In addition to this, graphene is employed in the form of graphene oxide (GO) and reduced graphene oxide (rGO) as active electrode material in supercapacitors. GO and rGO are also employed in the form of composites as active materials[36].

Graphene possesses the following properties that have attracted so much attention:

- Tremendous conductivity (6000 Scm^{-1})
- High charge mobility
- Light weight
- Large surface area ($2675 \text{ m}^2\text{g}^{-1}$)
- High mechanical strength
- High efficiency
- Low cost

1.5.2 Polymers:

Polymers evince pseudocapacitative behavior by undergoing the charging/discharging process via redox reactions. Conducting polymers have attracted attention for their employment as active materials for supercapacitor electrodes due the following properties they possess:

- Low toxic environmental impact
- Easy fabrication
- Exhibit high conductivities when doped
- High working potential window
- Low cost
- High values of capacitance
- Large surface area
- Low equivalent resistivity and conductivity

Unlike carbonaceous materials, only the surface is not entailed in the charging/discharging process, but the bulk of the polymeric material also gets involved. This results in high values of specific capacitance.

There are two species of doped polymers: n-doped and p-doped. In n-doped conductive polymers, electrons from the external circuit accumulate onto the polymeric film (active material) and cations from the electrolyte solution present transport to the polymer in order to counter the charge build-up and maintain net neutrality. In case of p-doped polymeric films as active materials, the reverse is seen; electrons are transported from the polymeric film to the external load applied[37]. This results in the transport of anions, from the electrolytic solution present, to the polymeric film in order to maintain net-neutrality.

Selecting a suitable working potential window is of utmost importance for conducting polymers as at high positive potentials, the conducting polymer degrades and at very low negative potentials, the polymer chain settles into an un-doped state; rendering the polymer an insulating film.

The following three types of polymeric materials are most commonly used as active materials for supercapacitor electrodes:

- Polyaniline (PANI)
- Polypyrrole (PPY)
- Poly (3,4-ethylenedioxythiophene) PEDOT

1.5.2.1 Polyaniline (PANI):

Polyaniline has gained a lot of research interest over other conducting polymers due to:

- Low cost
- Good redox reaction reversibility

- Stability in air and solution
- Easy to synthesize
- High specific capacitance
- Flexibility

Polyaniline (PANI) exhibits pseudocapacitive behavior as redox reaction sites serve for the energy storage mechanism. Polyaniline can only be p-doped.

A huge number of reports have been published on PANI with capacitances in the range of 30 Fg^{-1} to 3000 Fg^{-1} . It has been observed that dissimilar morphologies of PANI yield distinct values of specific capacitance. Research is being carried on different doping levels, morphologies and fabrication processes and their effect on specific capacitance of PANI as an active material for supercapacitor electrodes.

One of the main drawbacks of PANI is its poor cyclic stability and its ability to degrade at high potentials. Thus, it is usually combined with other materials such as CNTs to enhance its conductivity and stability. Polyaniline can be synthesized by polymerizing the aniline monomer with an oxidant such as iron chloride or ammonium persulphate or by applying potentials; this synthesis method is also called the electrochemical method[38]. Out of these two methods, the polymerization method prepares bulk quantity of polymer rapidly, but electrical polymerization results in high values of specific capacitance. An extraordinary specific capacitance value of 2093 Fg^{-1} has been proclaimed by Li et al. for electrochemical polymerization.

Polyaniline(PANI) possesses three different oxidation states:

- Emeraldine base (EB)
- Leucoemeraldine (LE)
- Pernigraniline (PE)

Out of these three, PANI-EB evinces highest stability and conductivity. Polyaniline is employed in supercapacitors, fuel cells and batteries.

1.5.2.2 Polypyrrole (PPY):

First synthesized in 1968, polypyrrole has been employed in multiple applications; such as:

- Biosensors
- Biocompatible polymers
- Microactuators
- Supercapacitors
- Batteries
- Coatings
- Chemical sensors
- Fuel cells
- Conductive adhesives

The advantages that prompt the useage of polypyrrole (PPY) as an active material in energy storage device are listed below:

- Good redox reactivity
- Ease of synthesis for large-scale production
- High conductivity
- Low density

The synthesis of polypyrrole consists of polymerization of the pyrrole monomer; followed by an oxidation step of the polymer. Chemical or electrochemical oxidation metamorphs the polymer polypyrrole into a conducting polymer. Polypyrrole undergoes oxidation reaction much easier in comparison with other conducting polymers[39]. It exhibits pseudocapacitive behaviour when employed as an active material in energy storage devices. Polypyrrole (PPy) stays well adhered to an electrode when the film thickness is less than 10 μm . In case the polypyrrole (PPy) film thickness is greater than 10 μm , the polymer film will scrape off of the electrode. This, in turn, degrades the function of the supercapacitor.

In comparison with polyaniline (PANI), the pyrrole monomer is expensive. In spite of possessing some good properties, polypyrrole also possesses some demerits such as:

- Low mechanical strength,
- Thermal degradation at temperatures higher than 150°C - 300°C
- Structural degradation after doping/de-doping

1.5.3 Metal oxides:

In supercapacitors, metal oxides are classified into transition metal oxides or noble metal oxides. Noble metal oxides, such as Ruthenium oxide (RuO_2) or iridium oxide (IrO_2) are famously known to evince excellent electrical conductivities along with superior power densities. However, large-scale application of these metals is not feasible; as ruthenium (Ru) and iridium (Ir) both belong to the platinum group of the periodic table i.e. they are rare metals. Their rarity and high cost recedes their employment for commercial production.

This is where transition metal oxides (TMO) come to be utilized. Metals, such as, nickel (Ni), manganese (Mn), cobalt (Co), etc. have abundant reserves in nature, and are used in oxide form as active materials for supercapacitor electrodes. Each transition metal oxide differs from others in crystallinity and redox behavior.

1.5.4 Metal sulphides:

On one side, metal oxides or metal hydro-oxides are obstructed by their:

- Low rate capability
- Low conductivity

And as previously mentioned, conducting polymers are also hampered by their:

- Low conductivity
- Poor cycling stability

These demerits obstruct their employment in a wide range of large-scale applications.

Whereas, recently, metal sulphides have gained a lot of research interest as active materials for supercapacitor electrodes owing to:

- Abundance in nature
- Multiple oxidation states
- Low electronegativity
- Electrochemically rich redox sites
- High specific capacitance
- Excellent electrical conductivity
- Low cost
- Good cyclic stability
- High energy density
- Excellent performance

Sulphide ions are known to possess flexible nanostructures. These structures promote fast electric charge transport along their crystal structure and have excellent electron conductivities. As sulphides possess more active and enhanced redox sites than oxides and conducting polymers, these materials have gained a lot of research potential. Explicitly, NiCo_2S_4 has gained a lot of interest and has been researched on comprehensively. Reportedly, compared to single metal sulphides, ternary metal sulphides have been evincing higher electrochemical performances; this ameliorated behavior can be attributed to the enhanced chemical redox chemistry of the sulphide material because of the presence of two different metals in the sulphide compound.

Currently, ternary metal sulphides have been gaining a lot of research interest for batteries and supercapacitor electrodes due to the chemical and electrical properties they possess. Ternary metal sulphides such as nickel cobalt sulphide (NiCo_2S_4), copper cobalt sulphide (CuCo_2S_4), manganese cobalt sulphide (MnCo_2S_4), etc. have evinced excellent capacitance and enhanced electrochemical performance due the fact that they possess multiple oxidation states and smaller band gaps.

Although, ternary metal sulphides have evinced ameliorated better electrochemical performance for electrochemical energy storage systems, their main drawback lies in the following two:

- Low rate capability
- Limited cycle stability

Now research is being carried out to overcome the challenges researchers face with ternary metal sulphides. This is necessary for their deployment in large-scale applications. There is a vast area of research in the domain of ternary metal sulphides in order to make chemically and mechanically better electrodes for energy storage systems such as batteries and supercapacitors. Researchers are also focusing on the architecture of these sulphide compounds where there is room for more improvement so that new architectures can be developed with enhanced electrochemical performance, more active

redox reaction sites, plenty channels for easy electron transport along the structure and enhanced structural stability[40].

This thesis research topic is focused of single and ternary metal sulphides and sees the comparison between their electrochemical performances as active materials for supercapacitor electrodes.

Supercapacitor applications:

Owing to its fast charging and discharging capabilities, long life-time and good cyclic stability, supercapacitors are excellent candidates to be applied in a extensive range of applications. Following are some of the applications where supercapacitors are being employed:

- Automobiles
- Low cost
- Robotics
- Photonics
- Spaceships
- Telecommunication systems
- Hybrid transportation
- Grid stabilization
- Consumer electronics
- Railway transports
- Memory storage system.

Chapter 2

2. Experimental methods

2.1 Synthesis routes:

The synthesis routes for the fabrication of nanomaterials can be characterized into the following two approaches:

- Bottom-up approach
- Top-down approach

Below, we see in detail these two approaches and their types.

2.2 Top-down synthesis route:

The top-down approach for material synthesis comprises of physically bulking down the bulk material into a nanomaterial; either using mechanical or chemical energy. A bulk material is first reduced to its powdered form and then further, this powdered form is reduced down into nanoparticles. This approach is preferred for large-scale synthesis of materials. Following are the types of top-down approaches that are employed for the synthesis of nanomaterials:

- Lithography
- Thermal ablation
- Laser ablation
- Exfoliation
- Milling
- Sonication

- Ultraviolet irradiation
- Photochemical reduction
- Sputtering
- Etching

In comparison with the bottom-up approach, the top-down approach is less preferred as the resulting product has more impurities, grain boundaries and phase defects.

2.3 Bottom-up synthesis route:

The bottom-up approach for the synthesis of nanomaterials is preferred as this synthesis route results in products with fewer structural defects as compared to top-down synthesis route. Also, this method has fewer impurities[41]. The desired product is synthesized via a chemical route i.e. a chemical reaction. Bottom- up approach has the following types:

- Sol-gel method
- Coprecipitation
- Hydrothermal synthesis
- Solvothermal synthesis
- Polymerization
- Aerosol process
- Spray pyrolysis
- Atomic deposition (MBE)
- Molecular deposition (MBE)

- Micro-emulsion method

Whereas, this synthesis route is cheaper and produces ultra-pure nanoparticles with a narrow size distribution, this method has its demerits; one of the major demerits is the difficulty in large-scale production. Also, the chemicals required for the synthesis need to be purified.

2.3.1 Sol-gel method:

The chemistry of this method is based on the idea of dissolving/dispersing a solid material in a liquid (hydration step) and bringing it back in a controlled manner. The colloidal particles or polymers stay agglomerated in a liquid phase forming a stable three-dimensional gel like network. Formation of a gel is better known as the dehydration process. After the hydration and dehydration step, thermal heating, either solvent evaporation or supercritical extraction, takes place which removes/evaporates the liquid and results in the final product. Sol, without undergoing the dehydration step, can also be heated; this is known as the gelation evaporation and results in sol fibers, powders or xerogel films. Generally, sol particles interact with one another via Van der Waal forces or hydrogen bonding. In most gel systems, the interaction between components is of covalent nature.

This method gains superiority over the co-precipitation method as it has high levels of homogeneity, whereas, inhomogeneous reactions result in co-precipitation.

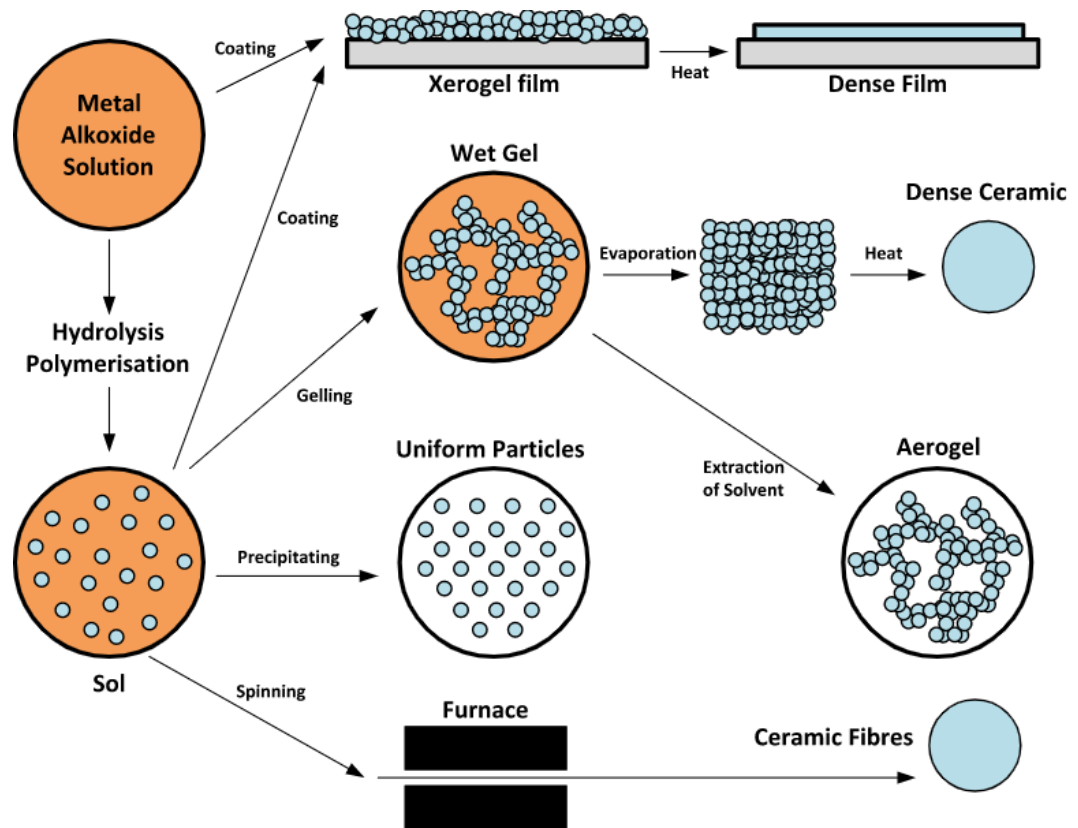


Fig. 2.1: schematic representation of sol-gel synthesis

The advantages of this method are listed as:

- Mixing at atomic level is possible
- Small, easily sinterable, particles are formed.
- Simple and low cost method
- Low temperature route
- High homogeneity is achieved
- Controlled stoichiometry of multi-component compounds
- Controlled hydrophobicity and hydrophilicity

The disadvantages of this method are listed as:

- Weak forces of interactions between components
- Porosity control is difficult

2.3.2 Hydrothermal/solvothermal synthesis route:

In a sealed vessel (or autoclave), chemicals mixed in an aqueous solution are poured. This sealed vessel is heated above the boiling point of the aqueous solution present and a chemical reaction results. Autogenous pressure is created by heating as the solubility of water increases with the increase in temperature. This method is based on the physics of temperature and pressure. This synthesis route follows the liquid nucleation model.

In case the chemical reaction is taking place in the presence of water as the aqueous solution, the method is referred to as ‘hydrothermal’, but in case the aqueous solution is some other solvent, the method is referred to as ‘solvothermal’.

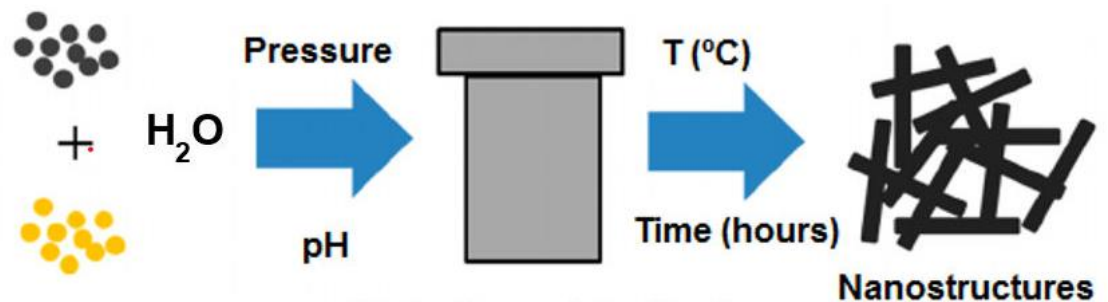


Fig. 2.2: schematic representation of hydrothermal synthesis

The advantages are listed as:

- Simple method
- Easy route
- Cheap method

- Morphology can be controlled by changing time, temperature, concentration of precursors and solvent present.

The disadvantages are listed as:

- Not for all materials
- Variation in size may be obtained
- Morphology and size may be difficult to control
- Safety issues

2.3.3 Co-precipitation synthesis route:

For the synthesis of nanoparticles, co-precipitation synthesis route involves the mixing of a cationic solution and an anionic solution. A homogeneous solution is prepared as supersaturation is a key step in this synthesis process; as it generates conditions for the nucleation to take place. Supersaturation conditions are achieved and thus, nucleation takes place. Tiny nuclei grow in size and eventually agglomerate under supersaturated conditions. These precipitates are insoluble species and are filtered, dried and calcinated in order to achieve the final product.

The purity of the precursor salts, concentration of the solution, pH conditions, ionic strength, etc. are some of the main features that influence the morphology and size of the particles.

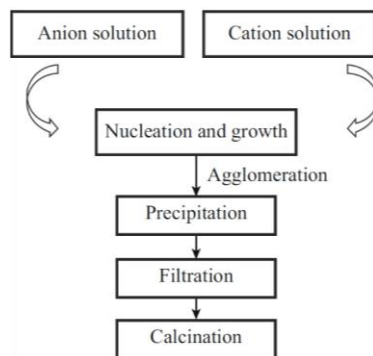


Fig. 2.3: schematic representation of co-precipitation route

The advantages are listed as:

- Large scale production
- Low cost method
- Environmentally friendly route

Disadvantages are listed as:

- Ostwald ripening/agglomeration
- Grain boundaries
- Wide size distribution of precipitates
- Controlling size of particles is extremely difficult

2.3.4 Microwave-assisted synthesis:

In this synthesis route, microwaves of frequency 2.45 GHz are most commonly employed. The major advantage of this synthesis is the homogeneous heating of the target solution as opposed to conventional heating of the target solution; this enables uniform nucleation of growth particles, narrow size distribution among the particles and faster crystal growth.

Microwaves are electromagnetic waves that oscillate at frequency in the range of 300 MHz to 300 GHz. The molecules of the target material are also oscillating at a particular frequency. When the microwaves are incident upon these molecules, the dipoles re-arrange themselves; resonance takes place and the dipolar molecules oscillate in-step with the incident microwaves. The more polar a molecule, the more strongly will it interact with the electric field of the incident electromagnetic microwave. Homogeneous heating of the target sample takes place because of the constant collisions and friction between molecules. Reportedly, particle size can be reduced by increasing time of irradiation; higher temperatures. Extremely low amount of by-products are

formed as the target temperature is instantly reached starting the chemical reaction and not providing enough time and energy for the by-products to get produced.

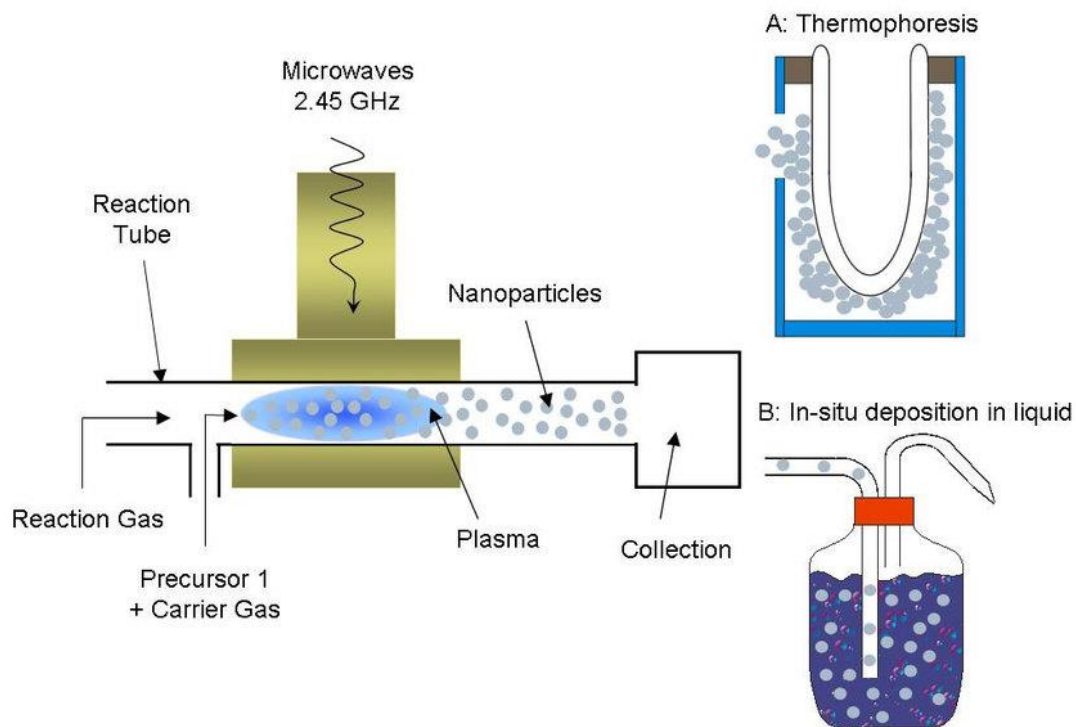


Fig. 2.4: schematic representation of microwave-assisted synthesis route

Advantages are listed as:

- Can be instantly switched on and off
- Green synthesis route
- Homogeneous heating
- Rapid energy conversion
- Higher product yield
- Products with high purity are formed

Disadvantages are listed as:

- Closed container can burst

- Solvent evaporation

2.3.5 Micro-emulsion synthesis route:

Micro-emulsion route is another synthesis method for the production of nanoparticles; in which two different phases are mixed together with one another via a chemical reaction. There are two types of micro-emulsion reactions; one is water-in-oil (W/O) where nano-sized aqueous droplets (e.g. water) are dropped in an oil bath and then, a surfactant is added to stabilize the foreign water droplet by creating a micelle or a reverse micelle structure (orientation depends on the composition of surfactant molecule). Another method is oil-in-water (O/W) which follows a similar route. The micellar structures act as nano-reactors for when two different micelles, each containing different reactants, come in contact with each other, the micelles may collide with each other. This is followed by coalescence of the micelles and eventually, mixing of the reactants they contain within.

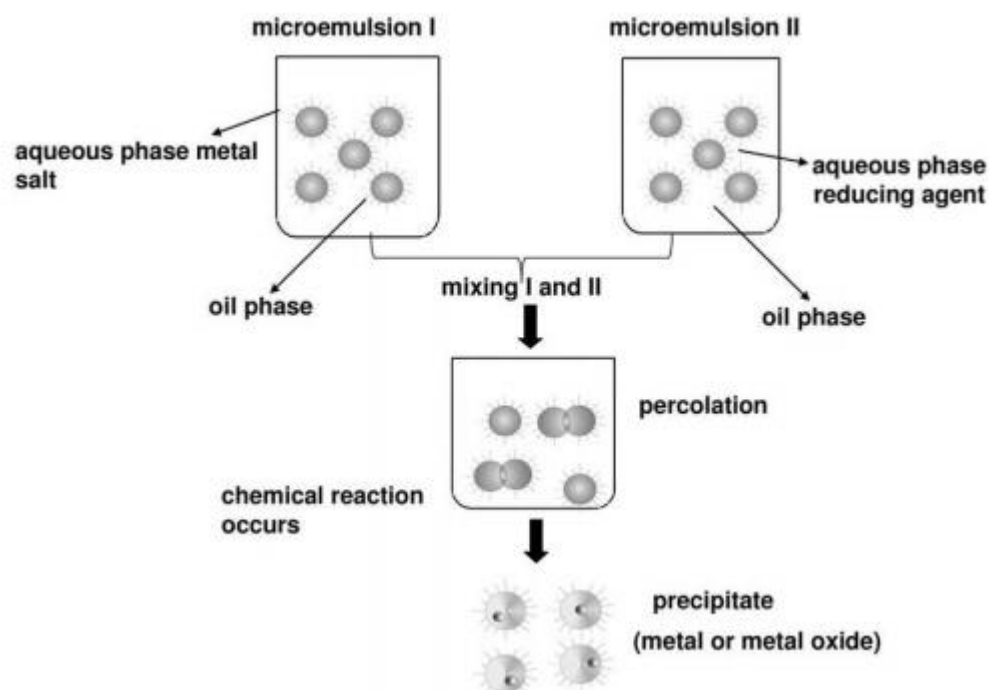


Fig. 2.5: schematic representation of micro-emulsion synthesis route

Advantages are listed as:

- Control over the size distribution
- Growth kinetics
- Properties can be controlled
- Shape, structure and composition can be controlled

Disadvantages are listed as:

- Surfactant removal is a challenge

2.3.6 Sonochemical synthesis:

This synthesis route is categorized under liquid-phase or wet chemical synthesis methods; where ultra-sonic waves are incident upon a liquid. This results in high temperatures that end up breaking chemical bonds. This phenomenon is called ‘acoustic cavitation’; cavitation is defined as the growth and abrupt burst of a bubble in liquid. The bubbles are where the word ‘cavity’ is derived from. The explosion of bubble form localized hot spots of extreme temperatures, for few nanoseconds; the temperature can usually reach around 5,000 K to 25,000 K and pressures around 20 MPa. The heat quickly dissipates and the spots undergo rapid cooling, obstructing the formation of crystalline structures; thus, resulting in the formation of structurally amorphous products.

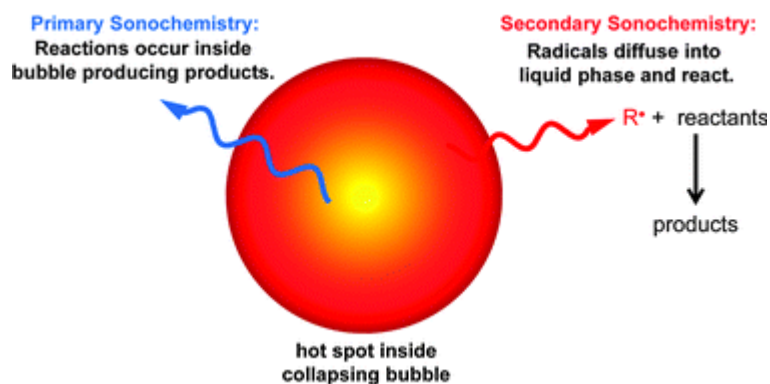


Fig. 2.5: schematic representation of sonochemical synthesis route

Advantages of this method:

- Small sized particles
- Amorphous products are produced
- Environmentally friendly
- Rapid reaction rates
- Small sized metal nanoparticles are easy to produce

Disadvantages of this method:

- Large-scale production is difficult
- Complex procedure

2.4 Aims and objectives:

The aim of this research is to synthesize mesoporous materials to be employed as active materials for electrodes in supercapacitors. Now, the objectives of this research are listed below:

- Synthesis of nickel sulphide (NiS) via hydrothermal route.
- Synthesis of nickel cobalt sulphide (NiCo₂S₄) via solvothermal route.
- Synthesis of zinc nickel cobalt sulphide via solvothermal route.
- XRD testing, SEM testing, FESEM testing and EDS testing of the three aforementioned synthesized sulphides.
- Electrochemical testing of all three synthesized sulphide compounds.
- Testing of these sulphides as active materials for electrodes in supercapacitors.

- Furthermore, these materials can be tested as electrodes for batteries.

Chapter 3

3. Literature review

In recent years, supercapacitors (or ultracapacitors) have attracted and enticed more regard from the researchers working on energy storage systems. For supercapacitor devices, their low energy density is the main problem; demanding to be improved on. Apart from this problem, recent advancements in the electrode material field of science and technology; they (the researchers) are filling in and minimizing the gap between the batteries and fuel cells.

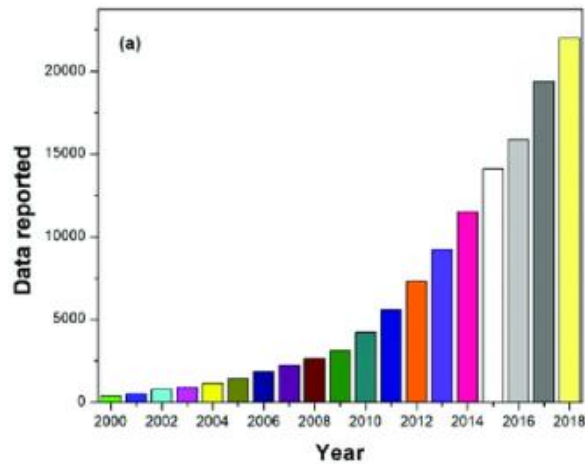


Fig. 3.1: Number of research publication on supercapacitors from the year 2000-2010

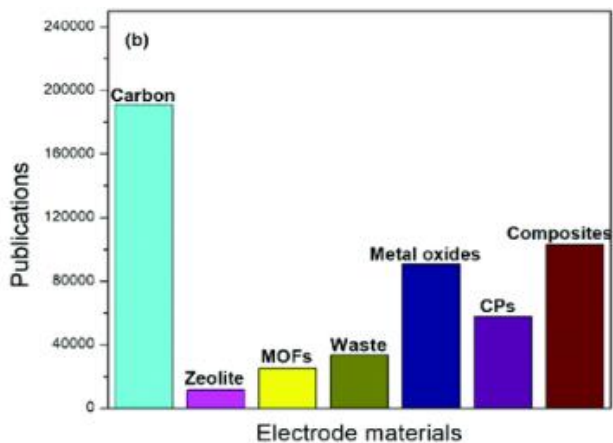


Fig. 3.2: Publications on electrode materials

The above figures 3.1 and 3.2 represent the amount of research work publications conducted and published in the field of supercapacitors as well as the materials being focused and researched/tested on in the last two decades.

Currently, due to the low cost, amazing redox reversibility, environmental friendliness, high theoretical capacity, excellent charge conductivity, nickel sulphide is being researched on by researchers as a promising material to be employed in energy storage systems.

Additionally, nickel sulphide is known for different morphologies and structures; each one poses a change in its properties. The phases researchers have come across are: NiS, NiS₂, Ni₃S₂, Ni₃S₄, Ni₇S₆ and Ni₉S₈. Some of these compositions and structures are complex and this complexity is attributed to the production/synthesis process; when the sulphur-rich phases are in more abundance as compared to the presence of the nickel-rich phases. Ni₃S₄ has gained much research interest due to its difficulty in existing in a single phase; it is known to mostly exist with a structure comprising the co-existence and crystallization with two different, but stable phases i.e. NiS₂ and/or NiS. This can be attributed to a sulphur-rich phase production.

In supercapacitor science, a lot of studies are currently being carried out based on the morphology, because capacitance is strongly dependent on morphology.

Wang et al. reportedly synthesized nanoframes of Ni₃S₄ with a rigid three dimensional structure for applications in pseudocapacitors. A simple solvothermal synthesis route was employed for the fabrication of Ni₃S₄ nanoframes. Electrochemical measurements of this structure exhibited excellent specific capacitance of 1213 F g⁻¹ at a current density of 2 A g⁻¹ with high rate performance. Such excellent values are attributed to the high surface area availability and rigidity of the 3D nanoframe structure[42].

Nandhini Sonai Muthu et al. published a paper in “Applied Surface Science”, in 2019, about a simple, one-step hydrothermal synthesis of Ni₃S₄ mesoporous nanostructures at different annealing temperatures. If the annealing temperature is kept

at 200°C, the Ni₃S₄ mesoporous nanoflakes exhibit a high surface area value of 73 m² g⁻¹. The electrochemical measurements reveal an excellent specific capacitance of 1184 ± 71 to 548 ± 9 F g⁻¹ at specific current densities of 5 to 40 A g⁻¹. The supercapacitor device is assembled in a symmetric fashion (i.e. both electrodes made from the same active material); this assembly results in a high value of energy density of 9 W h kg⁻¹ at a current density of 2 A g⁻¹ and a high value of power density of 4.6 kW kg⁻¹ at a current density of 40 A g⁻¹. Moreover, after 5,000 repeated charge/discharge cycles, 72% retention of the initial capacitance was observed[43].

Van Nguyen et al. in August, 2020 published an article in the journal of “metals and alloys” about a simple one-step solvothermal synthesis of mixed nickel cobalt sulfides. Reportedly, the mixed nickel cobalt sulfides evinced maximum specific capacitances of 2599.6 F g⁻¹ and 1345 F g⁻¹ at scan rates of 10 mV s⁻¹ and 2 A g⁻¹ respectively. After 3,000 charging-discharging cycles, 95% of its initial capacitance was retained[44].

In August 2018, Jinhyeon Kang et al. reported an article where he fabricated nickel sulphide via dip coating method with reportedly a maximum capacitance value of 897 F g⁻¹ at a current density of 1 mA cm⁻²[45].

Tai-Feng Hung et al., in July, 2019, reported an article in the “Chemical Engineering Journal” about the synthesis of nickel sulphide by laser irradiation and its application as an active material for supercapacitor electrode. At 10 ms⁻¹ scan rate, a specific capacitance of 3761 Fg⁻¹ was reported. Reversibility and rate capability of 1152 Fg⁻¹ at 100 mVs⁻¹ was also reported[46].

Jinhyeon Kang et al reported an article based on the alternate-dip-coating method for nickel cobalt sulphide and the maximum capacitance he reported was the value of 515.7 F g⁻¹ at a current density of 1 mA cm⁻²[47].

Xingxing He et al. reported in the journal of “Electrochimica Acta” about using the hydrothermal method for growing nickel cobalt sulphide nanoparticles on Ti₃C₂ MXenes. The compositions of nickel and cobalt were optimized to achieve the best

performance from the active material. $\text{Ni}_{1.5}\text{Co}_{1.5}\text{S}_4@\text{Ti}_3\text{C}_{2-5}$ evinced a specific capacitance of 166.7 mAh g^{-1} at the current density of 1 A g^{-1} , capacitance retention of 73.9% after an increase in current densities of 20 times[48].

Haoshan Nan et al. reported, in March, 2020, a paper in “journal of power sources” on the pseudo-capacitative behaviour of low crystalline nickel cobalt sulphide. At current density of 5 A g^{-1} , specific capacitance of 666.27 F g^{-1} is reported. Moreover, after 10,000 cycles, the capacitance retention of 65.29% is also observed[49].

Xingxing He et al. reported a paper in February, 2020 about growing nickel cobalt sulphide nanoparticles on Ti_3C_2 MXenes via a simple, one-step hydrothermal method. The assembled asymmetric device constituted of $\text{Ni}_{1.5}\text{Co}_{1.5}\text{S}_4@\text{Ti}_3\text{C}_{2-5}$ as the positive electrode with activated carbon as the negative electrode and evinced a high energy density of 49.8 Wh kg^{-1} at power density of 800 W kg^{-1} . Moreover, at 10 A g^{-1} , a capacity retention of 90% was observed at 8000 cycles[50].

Pengfei Cai et al. Reported, in February, 2020, an article in “Applied Surface Science” about the synthesis of hollow NiCo_2S_4 cages derived by ZIF-67 for high capacitance supercapacitors. A high specific capacitance of 1382 F g^{-1} at current density of 1 A g^{-1} was observed. Furthermore, the hollow NiCo_2S_4 cages and activated carbon was assembled in an asymmetric fashion which resulted in an energy density of 35.5 Wh kg^{-1} at a power density of 750 W kg^{-1} . Moreover, after 10,000 cycles, the cyclic stability of 79% retention rate was also reported[51].

Szu-Han Chou et al. in October, 2019, reported an article in the “Journal of Energy Storage” about how they employed electrodeposition for the growth of NiCo_2S_4 on a Ni foam. The active material was employed in a battery and a specific capacitance value of 1.75 F cm^{-2} at 5 mV s^{-1} was observed[52].

Ravindra N. Bulakhe et al., in March, 2020, reportedly published in “Materials Chemistry” for their 14th volume, NiCo_2S_4 nanoflowers synthesis on a Nickel foam via ionic adsorption and reaction. Excellent value of specific capacitance of 1899 F g^{-1} was reported at a scan rate of 5 mV s^{-1} along with 94% cyclic stability. Moreover, NiCo_2S_4

nanoflower structure evinced energy density of 55.16 Wh kg^{-1} at power density of the value 495 W kg^{-1} . Also, after 10,000 cycles, cyclic stability of 94% retention was reported[53].

Yue Zhao et al. reported an article in volume 108 of “Diamond and related materials” about the in-situ growth of NiCo_2S_4 nanoparticles on graphene via a simple, one-step solvothermal synthesis method. The electrodes were assembled in an asymmetric fashion with $\text{NiCo}_2\text{S}_4@\text{rGO}$ N-doped graphene electrodes and an excellent specific capacitance of 2418 F g^{-1} at a current density of 1 A g^{-1} was reportedly obtained. In addition, after 5,000 cycles, capacitance retention of 86.4% was obtained[54].

B. Joggi Reddy et al. Reported in volume 483 in “Applied surface science” in July, 2019, where they anchored Nitrogen doped graphene onto NiS nanoflakes via a hydrothermal process. The morphological analysis reveals the Nickel sulphide nanoflakes grown on a 2D nitrogen doped graphene. A specific capacitance value of 1120 F g^{-1} at a current density of 1 A g^{-1} . In addition, after 3,000 charge/discharge cycles, a good value of cyclic stability of 82% retention was reportedly obtained[55].

Jing Zhao et al. synthesized NiS via facial sacrificial template method employing $\text{Ni}(\text{OH})_2$ as a template. The structure of NiS changes from microflowers to microspheres with the increase in vulcanizing temperature. Electrochemical measurements taken revealed NiS-18 evinced a specific capacitance of 1315.4 F g^{-1} at 1 A g^{-1} current density[56].

In addition, at 10 A g^{-1} current density, after 5,000 GCD cycles, a retention rate of 89.2% was reported. Moreover, when NiS-18 was employed as positive electrode and activated carbon as a negative electrode (asymmetric device assembly), the energy density of 33.4 Wh kg^{-1} at 0.8 kW kg^{-1} power density was observed. The asymmetric device exhibited high cycling stability i.e. after 5,000 cycles, at 5 A g^{-1} current density, 87.3% retention rate was observed[57].

Uwamahoro Evariste et al., in June, 2020, reportedly published in volume 29 of “Journal of Energy Storage” about the electrodeposition synthesis of MoNiCoS on a

nickle foam. The specific capacitance of 1472 F g⁻¹ at 0.5 A g⁻¹. After 5000 cycles, an excellent cycling stability of 98% was measured[58].

Uwamahoro Evariste et al. additionally reported asymmetric supercapacitor assembly with MoNiCoS@NF as the positive electrode with AC/rGO as the negative electrode reportedly exhibited a high specific energy of 146.8 Wh kg⁻¹ at the specific power of 482.2 W kg⁻¹[59].

S. Nandhini et al., in August, 2018, reported an article in volume 449 of “Applied Surface Science” about the synthesis of NiS nanostructures for supercapacitors; via microwave-hydrothermal synthesis route. XRD patterns revealed different crystalline structures due to difference in synthesis procedures. Electrochemical measurements revealed a specific capacitance of 119 F g⁻¹ at a current density of 1 A g⁻¹ with energy density of 16.5 Wh kg⁻¹ and power density of 250 W kg⁻¹ respectively[60].

To Van Nguyen et al. reported a simple, one-step solvothermal synthesis of mixed nickel cobalt sulfides. The synthesized mixed nickel cobalt sulfides exhibited pseudo-capacitive behaviour and the electrochemical measurements revealed an excellent specific capacitance of 2599.6 F g⁻¹ at a scan rate of 10 mV s⁻¹; and at 2 A g⁻¹ current density, 1345 F g⁻¹ specific capacitance was reported. The mixed nickel cobalt sulfides showed better electrochemical performance than pristine NiS₂ and CoS₂. Moreover, the mixed nickel cobalt sulfide retained 95% of its initial capacitance value after 3,000 charge/discharge cycles[61].

Fuming Wu et al., in October, 2019, published in “Electrochimica Acta”, using a two-step hydrothermal synthesis route successfully fabricated zinc cobalt sulphide flowers on a nickel foam. The as prepared f-Zn_{0.76}Co_{0.24}S@Ni foam served as a binder free electrode for supercapacitor assembly and evinced an excellent specific capacitance value of 1906 F g⁻¹ at a current density of 1 A g⁻¹ along with excellent rate performance. Additionally, asymmetric supercapacitor device with f-Zn_{0.76}Co_{0.24}S@Ni foam and Fe₂O₃@rGO was assembled. The electrochemical measurements reported values of high energy density of 75.7 Wh kg⁻¹ at a power density of 700.5 W kg⁻¹. Moreover, after 8,000 cycles, superior cycling stability with 86.7% retention was displayed[62].

Tingting Ma et al. reported in the “Journal of Alloys and Compounds” about the facile synthesis via co-precipitation of $\text{Ni}_x\text{Co}_{1-x}\text{MoS}_y$ (NCMS). Different morphologies of Nickel cobalt molybdenum sulfide (NCMS) nanoparticles, nanorods and nanoplate-on-nanoparticles were obtained by adjusting concentration of NaOH in the ethanol-water solution poured in the autoclave for the hydrothermal step of a simple coprecipitation-hydrothermal synthesis route. The $\text{Ni}_x\text{Co}_{1-x}\text{MoS}_y$ active electrode material carrying nanoparticles and nanoplate-on-nanoparticles morphologies seemed to possess a higher available surface area for electrolyte penetration. Moreover, a huge number of pseudocapacitive active redox reaction sites were present for the charge-discharge process. In addition, The $\text{Ni}_x\text{Co}_{1-x}\text{MoS}_y$ electrode evinced a high specific capacity of 227 mAh g^{-1} at a current density of 1 A g^{-1} , excellent rate capability possessing 76.7% value for retention rate the current densities are increased from 1 A g^{-1} to 20 A g^{-1} ; after 1,000 cycles, at a current density of 5 A g^{-1} , high cyclability with 70.48% retention was observed[63].

In addition, for an asymmetrical supercapacitor assembly, $\text{Ni}_x\text{Co}_{1-x}\text{MoS}_y$ (NCMS) was employed as the positive electrode with active carbon as the negative electrode. Electrochemical measurements revealed an energy density value of 55 Wh kg^{-1} at a power density value of 850 W kg^{-1} (1 A g^{-1}). Such excellent results demonstrated the potential applicability of the $\text{Ni}_x\text{Co}_{1-x}\text{MoS}_y$ active material for supercapacitor electrodes in high-performance energy storage systems[64].

Haiyang Wang et al. reported, in 2018, a full-length paper in the “Chemical Engineering Journal” about rose-like structured Ni_3S_4 for employment in hybrid supercapacitors. The synthesis comprised of a simple, two-step hydrothermal route. Characterization revealed Ni_3S_4 owning a spinal structure and rose-like morphology. The Ni_3S_4 microflower structure exhibited excellent pseudocapacitive performance of $\sim 1797.5 \text{ F g}^{-1}$ at current density value of 0.5 A g^{-1} . In addition, for asymmetric assembly, the positive electrode was coated with Ni_3S_4 active material; while activated carbon (AC) served as the negative electrode. This assembly lead to electrochemical measurements that reported excellent value of energy density at $18.625 \text{ Wh kg}^{-1}$,

excellent power density of 1500.2 W kg^{-1} and good cycling stability; over 5,000 cycles, a high value of approximately 93% retention of the initial capacitance was observed[65].

Chapter 4

4. Material synthesis:

4.1 Apparatus required:

Following table lists the apparatus required for the synthesis method for this research:

☺	Teflon lined stainless steel autoclave (100 mL)
☺	Oven
☺	Nefarthum furnace
☺	Beakers
☺	Petri dishes
☺	Magnetic stirrer
☺	Weighing balance
☺	Vacuum filtration assembly
☺	Filter papers

Table 4.1: apparatus used for the synthesis process

4.2 Synthesis of Nickel Sulphide:

The starting materials for the synthesis of nickel sulphide are listed in the table:

Table 4.2: materials used for the synthesis of nickel sulphide

Chemicals	Purity level	Manufacturer
Nickle nitrate hexahydrate	97 %	DAEJUNG
Thiourea	98 %	DAEJUNG
KOH	97 %	DAEJUNG
Double-distilled water	99 %	VITRO DIAGNOSTIC Laboratory, Islamabad.

Nickel Sulphide Ni_3S_4 was synthesized via a one-step Hydrothermal synthesis route. The schematic representation of this easy one-step hydrothermal reaction is shown below.

Nickel nitrate hexahydrate ($\text{Ni}(\text{NO}_3)_2 \cdot 6\text{H}_2\text{O}$) and thiourea ($\text{CS}(\text{NH}_2)_2$) are added in 80mL of double-distilled water. This solution is placed under magnetic stirring at room temperature. In a separate beaker, 1M KOH solution is prepared separately and is then added drop-by-drop in the nickel nitrate and thiourea solution. The nickle solution is kept under constant magnetic stirring. KOH solution is added to maintain the pH of our solution at 10. Visibly, the addition of KOH enhances the opaqueness of the nickel nitrate hexahydrate and thiourea solution. This solution is magnetically stirred for 2 hours. The resultant solution has a light green colour to it.

The green solution is then decanted into a 100mL stainless steel autoclave and is tightly shut. The autoclave is then settled in an electric oven at 150°C for 6 hours. After 6 hours, the autoclave is cooled at room temperature to ensure all the desired reactions have taken place inside the autoclave. Black precipitates in the solution are a resultant of this reaction which are then filtered via vacuum filtration several times with double-distilled water. These black precipitates are then dried at 80°C for 24 hours in a vacuum oven. After drying, grinding is carried out using an agate mortar to crush the black

precipitates into fine powder. This product is then annealed at 200°C for 2 hours in a Nefarthum furnace.

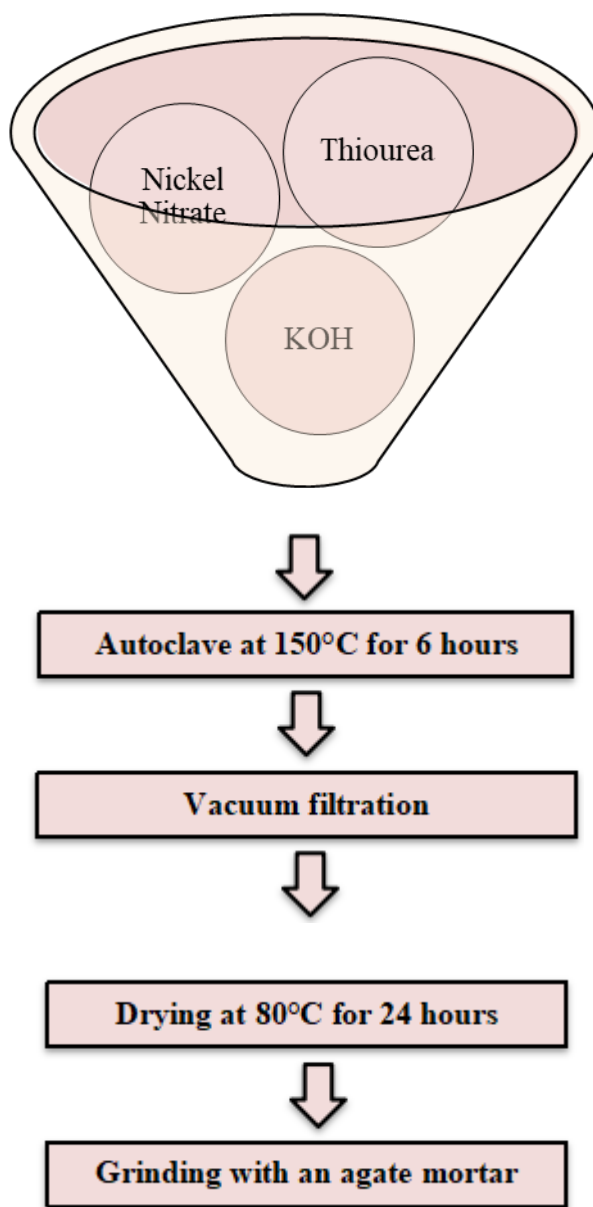


Fig. 4.1: Nickel Sulphide synthesis process flow

4.3 Synthesis of Nickel Cobalt Sulphide (NCS):

The starting materials for the synthesis of nickel cobalt sulphide are listed in the table below:

Table 4.3: materials used for the synthesis of nickel cobalt sulphide

Chemicals	Purity level	Manufacturer
Nickle nitrate tetrahydrate	97 %	DAEJUNG
Cobalt nitrate tetrahydrate	97 %	DAEJUNG
Thiourea	98 %	DAEJUNG
Double-distilled water	99 %	VITRO DIAGNOSTIC Laboratory, Islamabad.

One-step hydrothermal route was employed in the synthesis of NiCo_2S_4 . The schematic representation of the simple solvothermal synthesis route of nickel cobalt sulphide is presented below.

Nickel acetate tetrahydrate $\text{Ni}(\text{AC})_2 \cdot 4\text{H}_2\text{O}$ and $\text{Co}(\text{AC})_2 \cdot 4\text{H}_2\text{O}$ were added in a 40 mL ethylene glycol solvent and were magnetically stirred for half hour to ensue complete dissolution of reactants. After 30 minutes, thiourea ($\text{CS}(\text{NH}_2)_2$) is added and the solution is stirred on for another 30 minutes at room temperature. Once all the chemicals have achieved complete dissolution in ethylene glycol, the solution is decanted in a stainless steel autoclave and situated in the electric oven at 150°C for 26 hours. After 26 hours, the autoclave is cooled at room temperature to ensue complete reactions of reactants inside the autoclave. A solution with black precipitates is collected from the autoclave. This black solution is then filtered via vacuum filtration several times with double-distilled water and ethanol. The black precipitates are then dried at 60°C for 24 hours in a vacuum oven. Finally, the dried black product is grounded with an agate mortar.

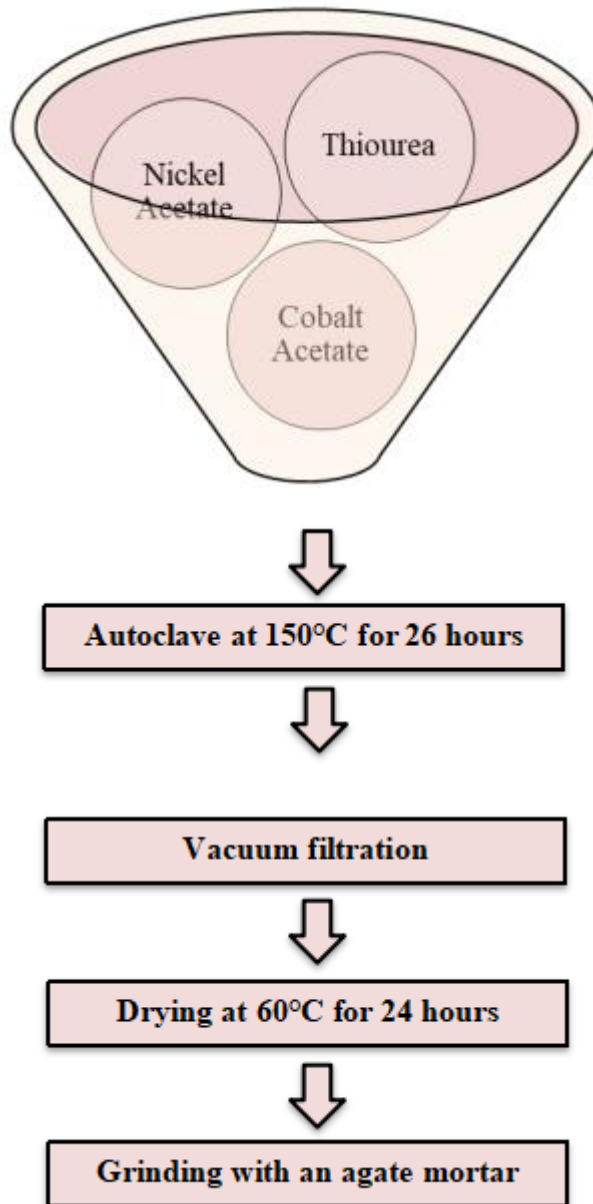


Fig. 4.2: Nickel Cobalt Sulphide synthesis process flow

4.4 Zinc Nickel Cobalt Sulphide (ZNCS) synthesis:

The starting materials for the synthesis of zinc nickel cobalt sulphide are listed in the table below:

Table 4.4: materials used for the synthesis of zinc nickel cobalt sulphide

Chemicals	Purity level	Manufacturer
Nickle nitrate tetrahydrate	97 %	DAEJUNG
Cobalt nitrate tetrahydrate	97 %	DAEJUNG
Zinc nitrate dehydrate	97 %	DAEJUNG
Thiourea	98 %	DAEJUNG
Double-distilled water	99 %	VITRO DIAGNOSTIC Laboratory, Islamabad.

Solvothermal synthesis technique was employed for the synthesis of zinc nickel cobalt sulphide (ZNCS). The schematic representation of this simple one-step solvothermal synthesis is presented below.

Nickel Acetate tetrahydrate $\text{Ni}(\text{AC})_2 \cdot 4\text{H}_2\text{O}$, Cobalt Acetate tetrahydrate $\text{Co}(\text{AC})_2 \cdot 4\text{H}_2\text{O}$ and Zinc Acetate dihydrate $\text{Zn}(\text{AC})_2 \cdot 2\text{H}_2\text{O}$ were added in 40 mL glycol ethylene solvent. This mixture was magnetically stirred on for approximately 40 minutes at room temperature. After a complete dissolution of Nickel acetate, Cobalt acetate and Zinc acetate, thiourea ($\text{CS}(\text{NH}_2)_2$) was added and magnetically stirred for another 40 minutes at room temperature. After stirring, the solution is decanted into a 100 mL stainless steel autoclave and situated inside an electric oven at 150°C for 26 hours. After 26 hours, the autoclave is retrieved from the oven and cooled at room temperature for a few hours to make sure the desired chemical reactions are completed. A solution containing black precipitates is the result of this reaction. This black solution is then filtered via vacuum filtration. A filter paper of 0.45 micro-meter pore size is employed in the filtration process. The black precipitates are washed several times with double-distilled water and ethanol. The obtained product is then dried in a vacuum oven at 80°C

for 26 hours to remove any leftover moisture. After drying, comes the simple step of grinding the black product into a fine powder. An agate mortar and pestle is employed for this purpose.

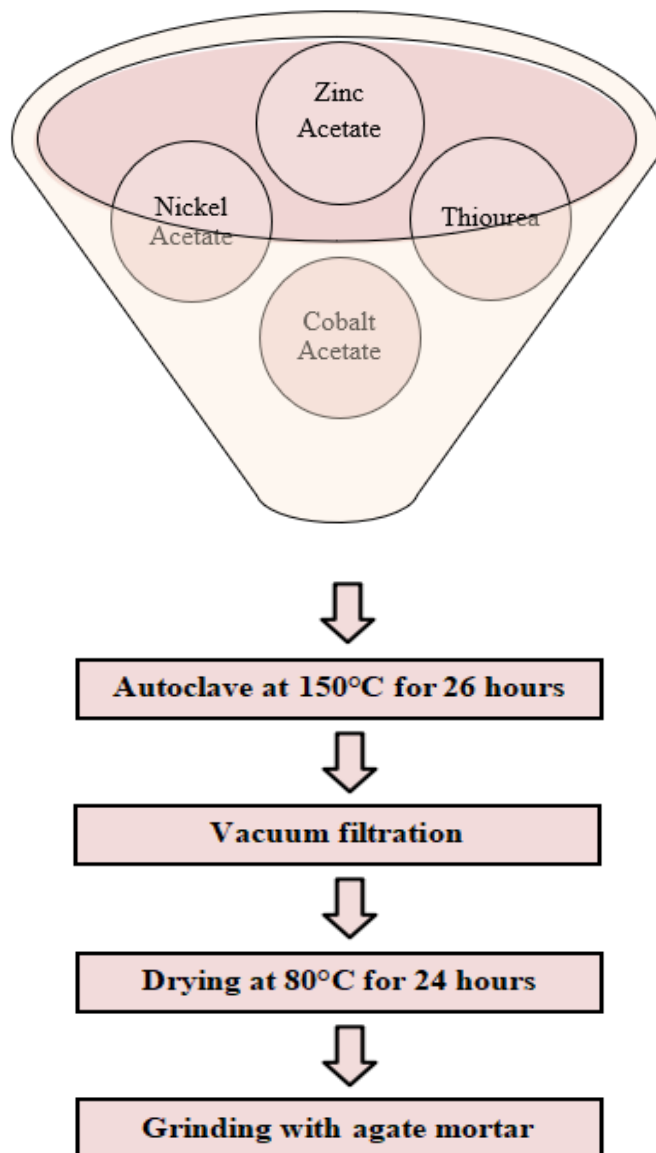


Fig. 4.3: Zinc Nickel Cobalt Sulphide synthesis process flow

Chapter 5

5. Characterization techniques

5.1 Scanning Electron Microscopy:

The Scanning Electron Microscope was founded in 1938 by Manfred von Ardenne. In summary, an emission of high energy electrons is utilized to create a 3D picture of the materials under examination with the resolution of up to 1 nm. As it comprises of electromagnets, one can control the degree of magnification. So as to be examined by a Scanning Electron Microscope (SEM) technique, the sample material must be conductive in nature while for insulator materials, the surface of the non-conductor material is covered with a slightly thin layer of conducting materials such as gold, graphite or aluminum.



Fig. 5.1: Scanning Electron Microscope (SEM) system

Construction and Working of SEM:

The vital modules of SEM include;

- Electron gun
- Electromagnetic lenses
- object chamber
- Secondary electron detector
- Display unit.

In this material analysis strategy, the fine light emission is engaged over a target material's surface. Photons or electrons are knocked off from the material's surface in the outcome. These knocked off electrons are then centered around the identifier[66]. The yield from the locator balances the brilliance of the cathode beam tube (CRT). For each point where the electron shafts are engaged and communicate, it is plotted on ensuing point on CRT and the material's picture is created.

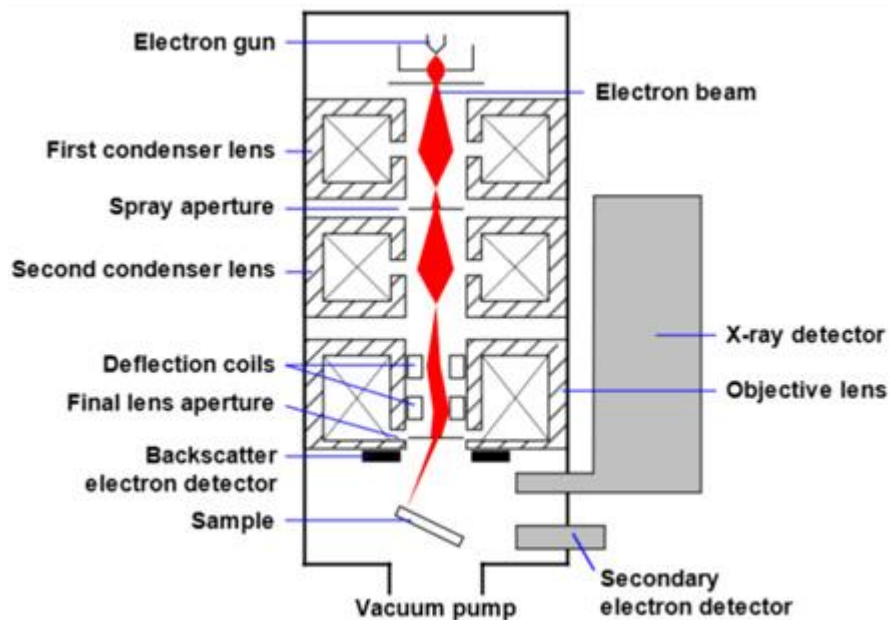


Fig. 5.2: schematic representation of a scanning electron microscope instrument

The electron-surface connection causes the arrival of auxiliary electrons; also known as secondary electrons (SE), X-ray beam and backscattered electrons (BSE).

Regular SEM mode for recognition is by means of secondary electrons. These electrons are produced from close proximity to the target surface. Thus, an articulated and clear image of the target material is obtained. It can uncover test detail even under 1nm in size. Likewise, versatile dissipation (elastic scattering) of incident electrons additionally happens and this results in the discharge of back scattered electrons. They rise up out of more profound and in-depth areas when contrasted with secondary electrons. Along these lines, their goals is similarly low. When an internal shell electron knocks off from its shell it radiates trademark x-ray beam.

We use SEM as it has simple arrangement and we can calculate our target material's morphology, chemistry, crystallography, and arrangement of planes. Amplification of SEM images can be controlled from 10 to 500,000 times[67].

Morphology of the target materials were analyzed on (JEOL-JSM-6490LA) and FESEM examinations were performed on (MIRA3 TESCAN). The element composition of the target material was dictated by EDS detector connected to FESEM.

5.2 XRD:

This gives exceptionally helpful data about distinguishing proof and evaluation of crystal phases, the dividing between crystal lattice planes and their separation scale and so on. The wavelength of X-beams is extending from 10 Å to 8 nm, however the frequency applied for the x-ray analysis lies in the range from 10 Å to 2.5 nm. Material sample for examination ought to be crystalline in nature, crystalline powders and leveled surfaces assigned to the categories of organic, inorganic, polymers, metals and diverse composite materials.

In 1912, Max Von Laue uncovered that X-rays were diffracted by the rigid solid crystals; this analysis had him getting a Nobel Prize[68].



Fig. 5.3: X-Ray Diffraction (XRD) system

The five general components of a X-ray diffractometer include:

- A radiation source
- Component to limit the wavelength of the receiving radiation beams
- Sample holder
- Radiation transducer
- Signal processing component
- Readout component

It is utilized for the crystal lattice structure verification of the material. It is a non-destructive strategy, and gives fingerprints of Bragg's reflection of crystalline

structured materials. It comprises of 3 principle parts. A cathode tube, test holder and a detector. X-ray beams are delivered by heating a metallic filament which ejects and accelerates electrons towards any target object material placed; the objective of the electrons is to slam into target material. A crystalline material is composed of several layers and planes. In this way, x-ray beams which possess a wavelength like these planes; i.e. their wavelength is equal to the distance between the lattice planes, is reflected at that angle of incidence is equivalent to the angle of reflection. "Diffraction" happens and it very well may be portrayed by Bragg's Law as:

$$2d \sin \theta = n\lambda$$

In 1912 W. H. Bragg and W. L. Bragg set up the above equation between dispersing/scattering angle, the separating distance between layers in a crystal structure (d-spacing) and wavelength of X-ray radiation utilized.

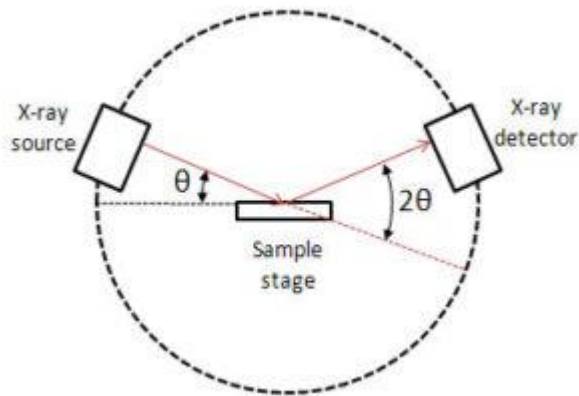


Fig. 5.4: Schematic arrangement of XRD Diffractometer components

Constructive interference happens as a result of when Bragg's law is fulfilled and "Bragg's reflections" will be detected and taken up by the placed detector. These reflection positions inform and enlighten us information concerning the inter-layer spacing; and the beam diffraction will enlighten us regarding the crystal phase, crystallinity, and target material purity[69]. By this strategy, one can likewise figure out the lattice mismatch, disengagements, dislocations, and unit cell measurements.

The most generally utilized objective material utilized for X-ray beam diffraction is copper with Cu-K α radiation = 1.5418 Å. The monochromatic X-ray beam is then focused to be incident to the target material sample. The unit used to manage and keep up the angle is called a goniometer. The most usually utilized detector is called a scintillation counter. The detector records the power of refracted X-beams gotten as a culmination of constructive interference of x-rays reflected off the crystalline planes[70]. Ordinarily, a X-beam diffractogram is calibrated at count per sec or intensity as a function of 2 θ degree with the scan range extending between ~5° to 90°. The total scan range of powder X-ray beam diffraction ranges from ~5° to 150°.

There are the following seven crystal system:

- Cubic (isomeric)
- Tertragonal
- Triclinic
- Orthorhombic
- Hexagonal
- Monoclinic
- Trigonal

X-ray diffraction analyses were performed by a STOE diffractometer at SCME, NUST.

5.3 Field emission scanning electron microscope (FESEM):

A FESEM is microscopic analysis element that acts by employing electrons (particles with a negative charge) rather than light. These electrons are effused by a field emanation source. The item is examined employing electrons accordingly via a crisscross pattern.

A FESEM is utilized to envision exceptionally minuscule topographical subtleties on the top layer or whole or fragmented objects. Analysts in science; biology, physics and chemistry, administer this strategy to scrutinize structures that might be as teeny tiny as 1 nanometer (= billion of a millimeter). FESEM might be deployed, for example, to examine organelles and DNA material in cells, synthetical polymers, and coatings on top of microchips.

Electrons are exuded from a field emission source and accelerated in the presence of a high electrical field gradient. Inside the high vacuum segment these supposed primary electrons are then, focused and redirected by electronic lenses to deliver a thin scan beam that strikes the target material. Therefore, secondary electrons are radiated from each speck on the target material. Angle and speed of these secondary electrons established with the surface anatomy of the target material. A detector captures the incoming secondary electrons and in turn, generates an electronic sign[71]. This received signal is amplified and changed into the form of a video scan-picture that is easily viewed on a screen or to a computerized picture that is saved and processed later.

5.3.1 Source of electrons:

In standard electron microscopic instruments, electrons are generally created by warming a tungsten fiber using methods for a current to a temperature of about 2800°C. Intermittently, electrons are generated using the Lanthanumhexaboride (LaB6) crystal; which is situated on top of a tungsten tendril. This adjustment verdicts in a higher density in the electron beam; what's more, a superior resolution than with the conventional gadget. In a field emission (FE) scanning electron microscope instrument, no warming yet an alleged "cold" source is utilized.

An amazingly slender and sharp tungsten stylus (tip breadth: $10^{-7} - 10^{-8}$ m) capacities as a cathode before a primary as well as a secondary anode. The voltage among cathode and anode lies in the confines of 0.5 to 30 KV. Since, the produced electron beam delivered by the FE source is approximately a thousand times less than in a customary microscope; the picture quality is chiefly superior. As field emission entails an outrageous vacuum (10^{-8} Torr) in the segment of the microscope, a gadget is at one's

disposal that constantly purifies the electron source by a current blaze. Rather than an ordinary tungsten filament, a FE tip lasts speculatively for a lifetime, given the vacuum is kept an eye on to be kept anchored.

5.3.2 Segment with lenses and apertures:

Using a set of electromagnetic lenses, an electron beam is focused (condenser and objective lenses, stigmator curled wires and scan coils) and the apertures in the segment to a little sharp spot.

5.3.3 Condenser lens:

The diameter of the electron beam is decided by the current in the condenser: a small diameter of the beam is a result of a low value of current; in the same fashion, a bigger glint is a consequence of a higher current. An attenuated thin beam has the favorable position that the resolution of the image is preferably superior, yet the deficiency that the signal to noise proportion is more awful. The circumstance is turned around when the electron beam has a huge measurement of its diameter. The condenser lens comprises for the most part out of two sections.

5.3.4 Scan coils:

In a zig-zag manner, the scan coils redirect the incident electron beam over the specimen. This scan movement results in the appearance of an image on the digital screen; the image carries information about the specimen. In addition, the amount of noise in the picture and the refreshing rate on the digital monitor is dependent of the scan velocity of the incident electron beam; a rapid scan rate equals a rapid refreshing which in turn, equates to a low signal which aids in much noise in the image. At a constant window size, if the scanned region on an object is really small, the magnification becomes large. At low magnification, for the prevention of a circular shadow, the employed scan coils often are in possession of lower and upper coils.

5.3.5 Objective lens:

The most bottom placed lens in the section is the objective lens. The objective lens centers the incident electron beam on the specimen. When the working distance is small (object placed at a higher point, that is nearer to the objective lens), the objective lens demands to exert a more prominent power in an attempt to avert the incident electron beam. The briefest working distance delivers the littlest gleam distance across, the best resolution, yet in addition the least fortunate depth of field. (The depth of field shows that extend vertical way in the specimen can even now is imaged pointedly).

5.3.6 Stigmator coils:

The stigmator curled wires are employed in order to address abnormalities in the x and y redirection of the incident electron beam and in this way, in order to acquire a totally round-molded electron beam. At the point when the incident electron beam isn't roundabout, yet ellipsoidal, the picture looks obscured and extended.

5.3.7 Image formation:

At the point when the primary electron beam assaults the target material, secondary electrons get ejected from the surface of the target material with a specific velocity that is controlled by the height points and different angles at the top layer of the target material. The secondary electrons, which are pulled in by the Corona, bombard and hit the scintillator (fluorescing mirror) that results in the production of a number of photons. The area and intensity of light of the mirror, shift hingeing on the attributes of the secondary electrons. The signal attributed by the scintillator is intensified; amplified, and transduced into a video signal that is taken care of to a cathode beam tube in synchrony with the examine mobility as for the incident electron beam. Difference in the 'original' picture that pops on the digital display monitor mirrors the morphological structure on the outer layer of the specimen under study. Corresponding to the simple picture, an advanced picture is produced which can be additionally processed for study.

5.4 Electron dispersive spectroscopy (EDX):

In order to study in great detail the elemental composition of a target material, energy dispersive X-ray beam spectroscopy (otherwise called EDS, EDX, or EDXA) is a

ground-breaking method that empowers the client to dissect the natural arrangement of the aforementioned material. The major working rule that permits EDS to work is the range of high vitality possessing electromagnetic radiation (X-beams) to discharge 'center' electrons (electrons that are not located in the peripheral outermost shell) from any atom). This guideline is known as Moseley's Law, which established that there was an immediate connection between's the frequency of light discharged and the nuclear number of the atom.

Expelling these electrons from the atomic framework will abandon a cavity that a higher energy possessing electron can fill in, and it will discharge energy as it becomes stable. The energy discharged during this stabalizing procedure is special to every element in the periodic table, and as such striking a target material with X-beams can be utilized to distinguish what elements are possessed by the target material, just as to what is the quantity they are available in[72].

Appeared beneath is a case of how EDS functions. The letters K, L, and M represents to the value of n ; that electrons in that particular atomic shell are present (K electrons, nearest to the core, are referred to the value of $n=1$ electrons), while α and β show the size of their transition. The stabalization from M to L or L to K are hence portrayed as $L\alpha$ or $K\alpha$; also, jumping from M to K would be referred to as a $K\beta$ transition. The method that is utilized for depicting these procedures in general are known as Siegbahn documentation.

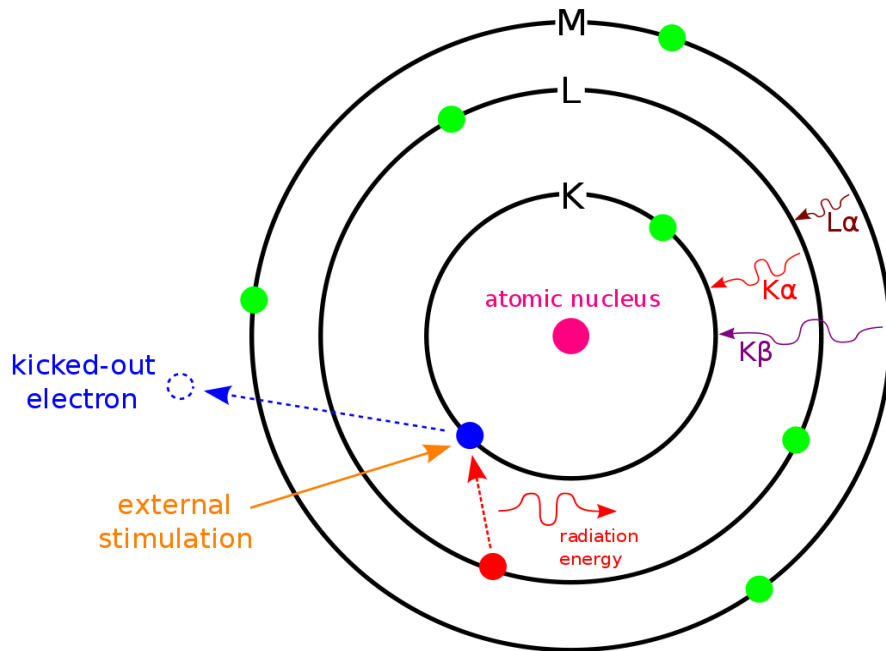


Fig. 5.5: Schematic representation of x-ray emission

XPS instrumental setup:

XPS instrument consist of

- X-rays source
- An electron energy analyzer
- Ultra high vacuum (UHV)
- Magnetic field shielding
- Detectors & computer system

UHV is utilized to expel surface tainting this will enhance the mean free path of electrons. XPS is utilized to study polymers, ceramics, metals and inorganic mixes. However, inorganic compounds are not, for the most part, investigated on the grounds that due to the high energy of x-rays, they degrade over time. XPS is utilized to quantify the accompanying:

- Chemical state

- electronic state
- Empirical formula
- Line profiling
- Depth profiling
- Elemental composition on material's surface
- Surface contamination

5.5 Electrochemical Analysis:

Electroanalytical techniques include the examination of an analyte by estimation and calculation of current and voltage in the electrochemical cell. Three essential sorts are:

- Voltammetry
- Coulometry
- Potentiometry

Potentiometry includes the estimation of cathode potential. Coulometry includes the estimation of current as a function of time and volumetric examination is a calculation of current as a component of voltage. By and large, measurements are carried out in an electrochemical cell containing three sorts of terminals serving as electrodes as appeared in the following figure shown below:

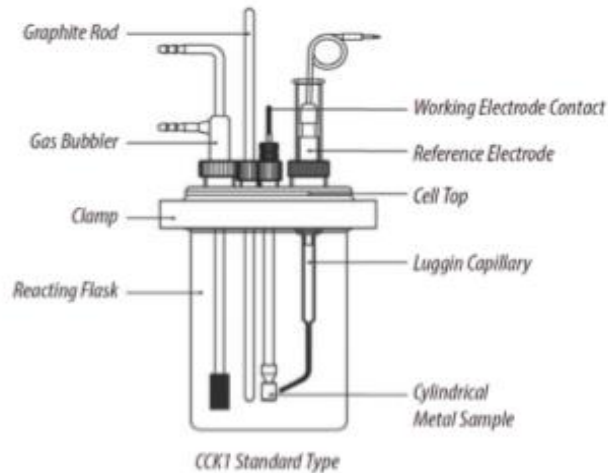


Fig. 5.6: Schemetic representation of an Electrochemical workstation electrode assembly

At School of Chemicals and Materials Engineering (SCME), NUST, a Biologic VSP is the research-grade potentiostat used for electrochemical analysis. Gear comprises of the following:

- Work station
- Electrochemical cell
- Programming framework
- PC equipment.

It is employed for many applications including the following mentioned:

- Battery testing
- Fuel cell
- Bio-fuel cell
- Liquid conductivity
- Electrochemical deposition of a thin-film
- Material impedance spectroscopy

- Corrosion testing
- Sensors
- Photovoltaics
- Capacitor and supercapacitor testing

For the most part, Ag/AgCl and standard hydrogen electrode (SHE) are utilized as a reference terminal. Capability of the other two different electrodes is estimated comparative with the reference terminal. Counter electrode is the one that completes the electrical circuit. It permits the flow of mobile electrons from working electrode to counter terminal and thus, the current is estimated. Platinum wire, gold or carbon-based counter electrodes are normally utilized for examination. The counter electrode terminal, otherwise called an auxiliary electrode, is a current directing anode fundamental for culmination of a circuit in an electrochemical cell. Since, the reference terminal has a fixed potential value; in this manner, any variation (redox process) in the cell is because of the other two conductive terminals. For an electrode to go about as a counter terminal, it must fulfill certain conditions:

- Reaction by-products formed at the counter electrode must not react chemically at the working electrode.
- The electrode should not dissolve in the electrolyte present in the electrochemical cell.
- In order for the electrode area to not affect the limiting current, the area of the counter electrode must be larger than that of the working electrode.

The counter electrode terminals ordinarily comprises of a platinum wire and much of the time, carbon electrode terminals. In the current research work being carried out, carbon electrodes have been utilized as a counter terminal[73].

In the analysis working window, the working electrode terminals are electrochemically inert. Intriguing reactions take place over the working electrode. In

electrochemical analysis system, the most generally utilized working electrode is the glassy carbon electrode (GCE).

On this electrochemical potentiostat, supercapacitor testing performed includes:

- Cyclic Voltammetry (CV)
- Galvanostatic Charge-Discharge (GCD)
- Electrochemical Impedance Spectroscopy (EIS)

5.6 Cyclic Voltammetry:

Cyclic Voltammetry (CV) is an electrochemical procedure which gauges the current that enkindle in an electrochemical cell, over the stipulations where voltage is in abundance of that preceded via Nernst equation. CV is effectuated by cycling the potential of a working electrode terminal, following by estimating the ensuing current.

Instrumentation:

A CV framework comprises of an electrolysis cell, a potentiostat, a current-to-voltage converter, and an information obtaining framework. The electrolysis cell comprises of the following:

- Working electrode terminal
- Counter electrode terminal
- Reference electrode terminal
- Electrolytic solution

As the reference electrode terminals keeps up a steady potential, the potential of the working electrode terminal changes linearly with time. The counter terminal is set to conduct current from the sign source to the working terminal. The reason for the electrolytic arrangement is to feed ionic beings to the electrode terminals during oxidation and reduction processes. A potentiostat is an electronic gadget which utilizes a

dc power source to create a potential which can be kept up and precisely decided, while permitting little flows of electricity to be brought into the framework without changing the voltage[74]. The current-to-voltage converter quantifies the subsequent current, and the information procurement framework creates the subsequent voltammogram.

Most normally utilized Reference Electrodes are saturated calomel electrode (SCE) terminals and Silver/Silver chloride (Ag/AgCl). The counter electrode terminal is, for the most part, Platinum. The reason for the electrolyte is to give off ionic bodies. An electrolyte must have great conductivity. In supercapacitors, various materials evince various reactions. EDLC provides a rectangular bend curve though pseudo capacitor exhibits oxidation and reduction bump during forward and reverse cycle evinces redox reactions happens as shown in the following figure:

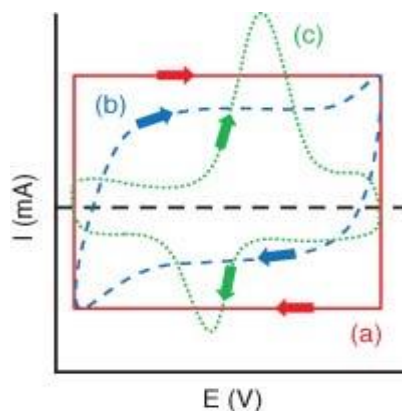


Fig. 5.7: Cyclic voltammogram curves of (a) ideal capacitor, (b) EDLC , and (c) pseudocapacitive materials

Now, in order to examine subjective data about electrochemical procedures under different conditions, CV can be utilized, e.g., reversibility of a reaction or the presence of intermediates in redox reactions. CV can likewise be utilized to decide the electron stoichiometry of a framework, the diffusion coefficient of an analyte, and the conventional decrease potential, which can be utilized as a distinguishing proof[75]. What's more, since the concentration is relative to current in a reversible, Nernstian framework, concentration of an obscure solution can be dictated by creating an adjustment curve of current versus concentration.

5.7 Galvanostatic Charge-Discharge (GCD):

GCD is the most widely recognized technique to test the charge and discharge property of the supercapacitors just as batteries. In GCD, measure the potential as a function of time at a steady current. One charge and discharge of the material is equivalent to one complete cycle. Like CV, GCD bends of EDLC and Pseudo capacitor is not similar. EDLC materials In EDLC type of supercapacitors, the charging-discharging cycles exhibit direct curve with almost no IR drop though if there should arise an occurrence of Pseudo capacitors the curve isn't straight and IR drop is huge in examination with the EDLC. This deviation alludes to the charge stockpiling component which happens because of the oxidation-reduction reactions. So also the straight reaction evinces that charge storage component isn't faradic implies that just physical charge storage takes place. GCD curves of both EDLC also, Pseudocapacitor is depicted in the following figure:

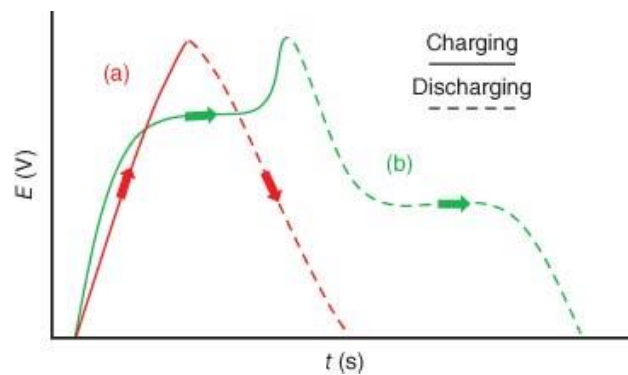


Fig. 5.8: GCD curves of (a) EDLC (b)Pseudo capacitor

The GCD strategy is very unique in relation to cyclic voltammery on the grounds that in this procedure the current is controlled and measurement of voltage is carried out. The GCD approach is one of the most extensively utilized electrochemical strategies and it has the potential of extension from lab usage to industrial range[76]. This methods are additionally a few times termed as chronopotentiometry also, it gives a knowledge of the accompanying boundaries, for example:

- Resistance
- Capacitance

- Stability

The function of GCD depends upon the use of a current pulse to the working electrode terminal (WE) and the quantification of output potential as a function of time. The difference of voltage in a GCD test is represented by the accompanying condition:

$$C = I\Delta t\Delta V$$

Where,

$\Delta V(t)$ = variable voltage, as a function of time

R = internal resistance

C = capacitance

I = current

Thus, looking at the above equation, it is clearly conspicuous that capacitance 'C' can be easily calculated by using slope of the GCD curve[77].

5.8 Cyclic stability:

Cyclic stability is one of the fundamental tests of energy storage gadgets. Cyclic behaviour of supercapacitors is tried and executed by numerous charging and discharging cycles. On a laboratory scale, ordinarily 500 to 10000 charging-discharging cycles were carried out to look at the capacitance retention of the target material.

Chapter 6

6. Results and discussion

6.1 X-ray diffraction (XRD):

The structural study of the synthesized materials were performed by powdered X-ray diffraction machine; with a step scan of 0.04° and scan rate of 1.00 seconds.

XRD was performed on the samples in order to examine the structural and compositional analysis of synthesized Nickle Sulphide (NS). The results gathered from the XRD analysis endorses the formation of the homogeneous cubic structure of Nickle Sulphide (NS) in complete agreement with JCPDF card 03-065-3103. There are no peaks of any type of impurity observed in the XRD pattern of Nickle Cobalt Sulphide and Zinc Nickle Cobalt Sulphide.

XRD analysis was performed to determine the crystal structure of prepared materials. All the diffraction peaks correspond well with JCPDF card 03-065-3103. Crystal structure belongs to the cubic and space group of Fd-3m. Diffraction peaks are slightly shifted in comparison to reference pattern because of difference in the atomic radii of Zn, Ni, and Co, but no change in crystal structure and no extra peaks are observed which means that sample is pure having (021), (300), (110), (220), (402) and (440) planes. However, (300), (220) and (402) are sharp peaks. The crystallite size of ZNCS was calculated by using the following formula:

$$D = \frac{0.9\lambda}{\beta \cos \theta}$$

Where θ is the angle of the diffracted peak, β is FWHM, and λ is the wavelength.

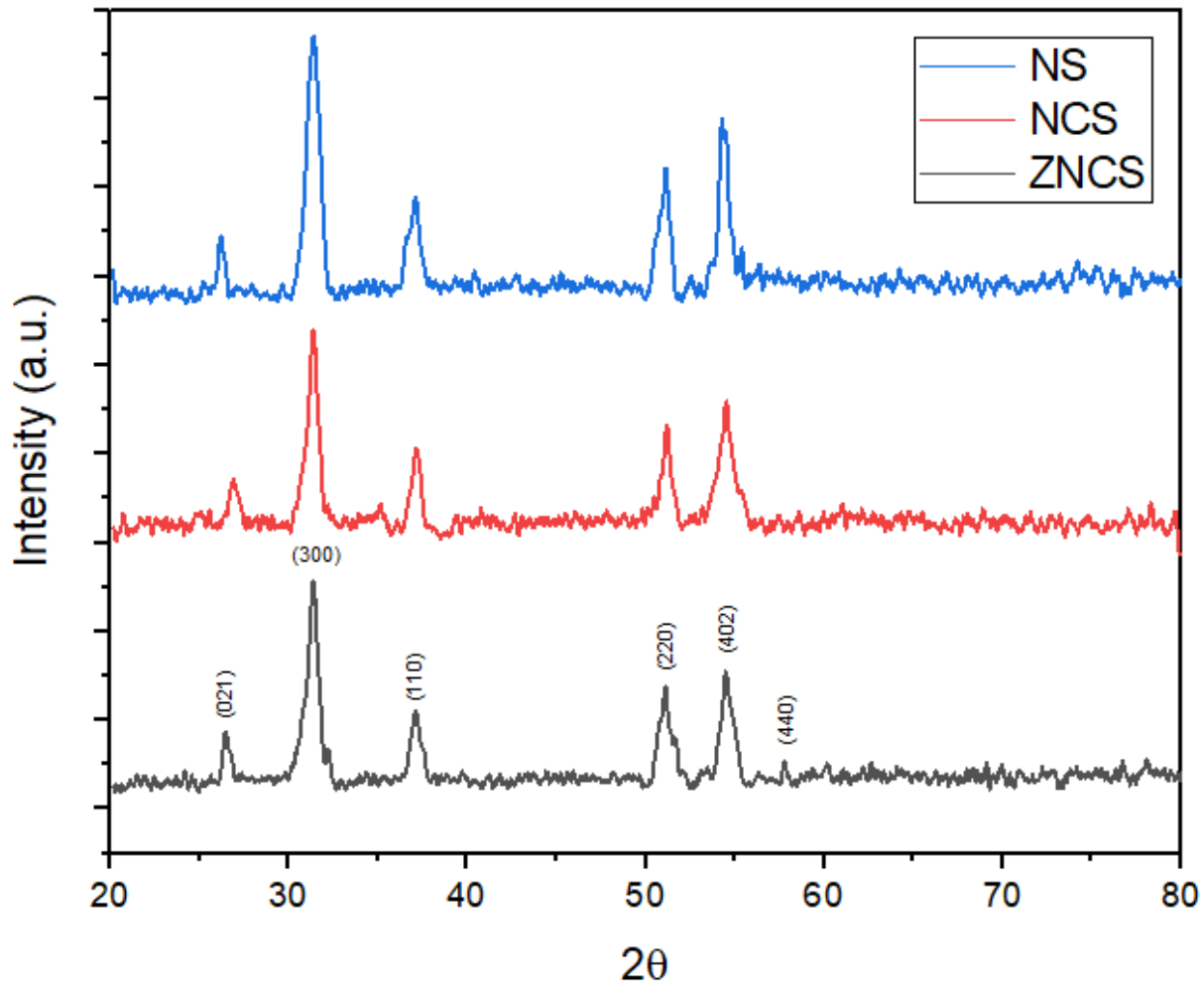


Figure 6.1: XRD spectrum of NS, NCS and ZNCS

6.2 Field emission scanning electron microscope (FESEM):

Morphology of Zinc Nickle Cobalt Sulphide (ZNCS) was examined by scanning electron microscope (SEM). SEM analysis of ZNCS evinces the nanoparticle nanostructures. Nanoparticles are arranged forming the structure which affirmed the porous nature of the material as well as high transport of electrolyte during the cycle of an electrochemical performance. Nanoparticle structure is conspicuously visible in Figure 6.2.

In addition, FESEM analysis were also carried out at Institute of Space Technology (IST).

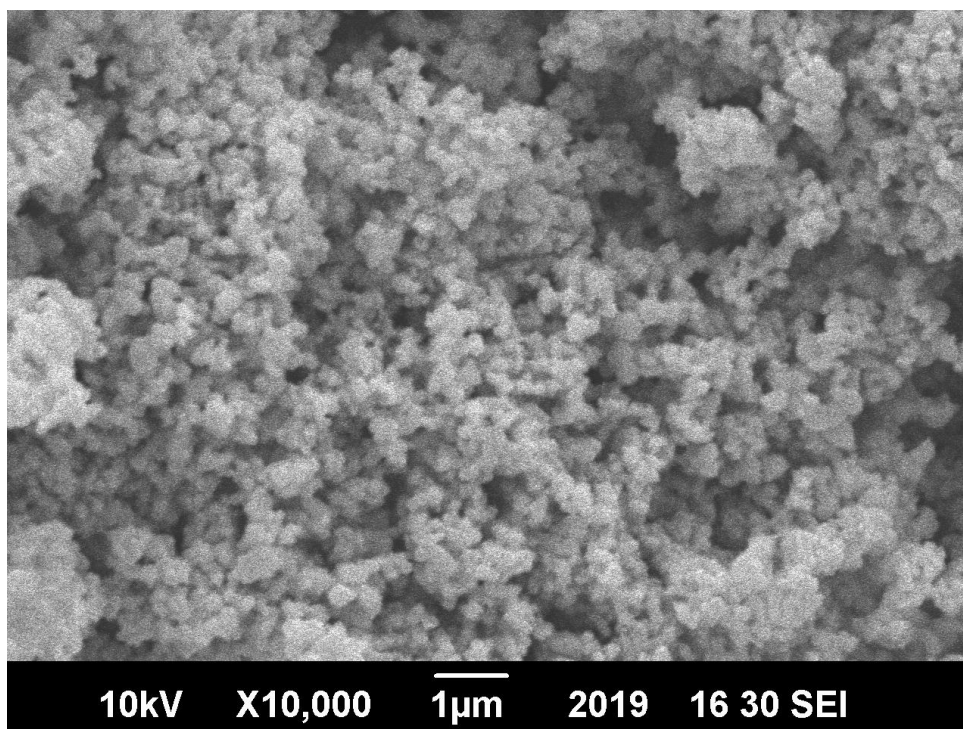


Figure 6.2: SEM of Nickel cobalt sulphide

FESEM shows Hierarchical Nanoparticles structure of Zinc Nickel Cobalt Sulphide in Figure 6.3. The nanoparticle arranged structure of Zinc Nickel Cobalt Sulphide (ZNCS) affirmed the fast charge transport methodology by permitting the pass-through of electrolyte more efficiently, and the transport of rapid ions evince better electrochemical performance the diameter of nanoparticles ranged from 75 nm to 90 nm forming a porous network.

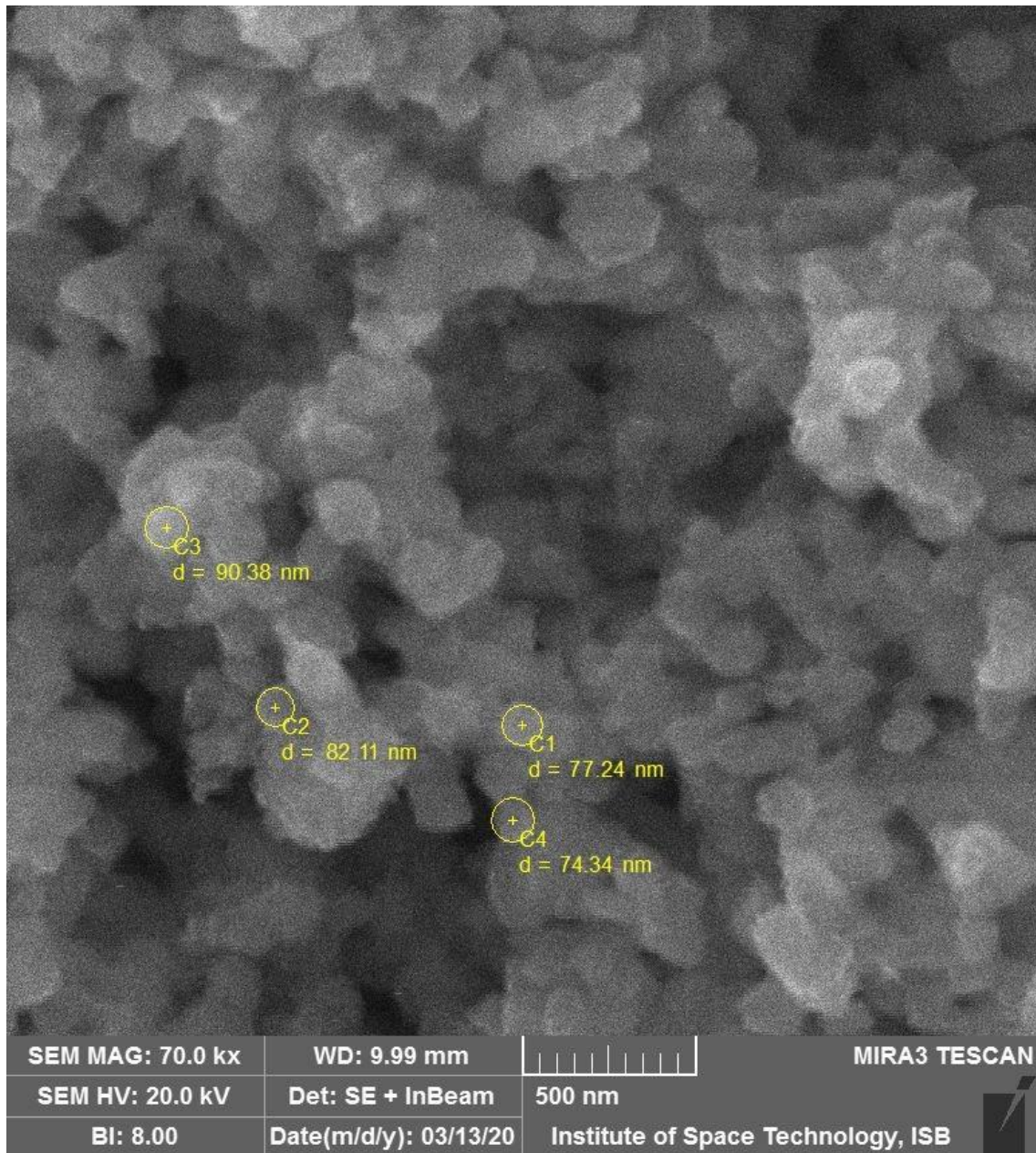


Figure 6.3: FESEM analysis of Zinc Nickle Cobalt Sulphide

To examine the morphology of nickel cobalt Sulphide (NCS), FESEM analysis was carried out as shown in Figure 6.3. Nickle cobalt sulphide also evinces hierarchical nanoparticle structural arrangement; which was similar to the Zinc Nickle Cobalt Sulphide (ZNCS). The nanoparticles formed are arranged hierarchically. The average diameter of nanoparticles of Nickle cobalt sulphide lies between 73 nm to 85 nm. Porous structure of Nickle cobalt sulphide was also affirmed by the FESEM images which means that charge transport mechanism was enhanced.

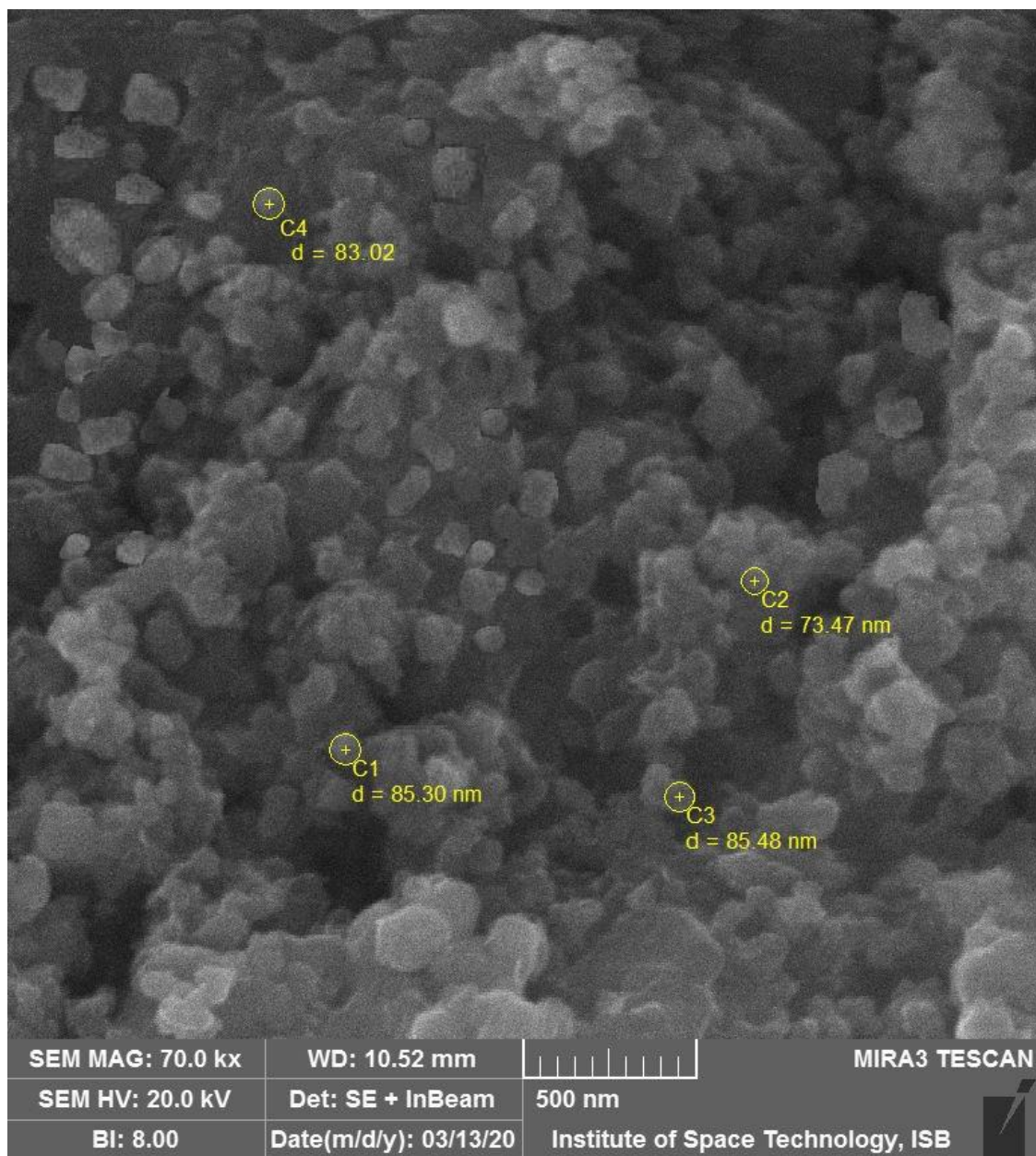


Figure 6.4: FESEM analysis of Nickle cobalt sulphide

In order to examine the morphology of nickel sulphide (NS), FESEM analysis was carried out. Nickle Sulphide (NS) also evinces hierarchical nanoparticle arrangement; which was similar to the Zinc Nickle Cobalt Sulphide (ZNCS) and Nickle Cobalt Sulphide (NCS). The nanoparticles are arranged in a hierarchical pattern. The average diameter of nanoparticles of Nickle Sulphide (NS) range between 82 nm to 91 nm. Porous structure of Nickle Sulphide was also affirmed by the FESEM images which means that charge transport mechanism was modified.

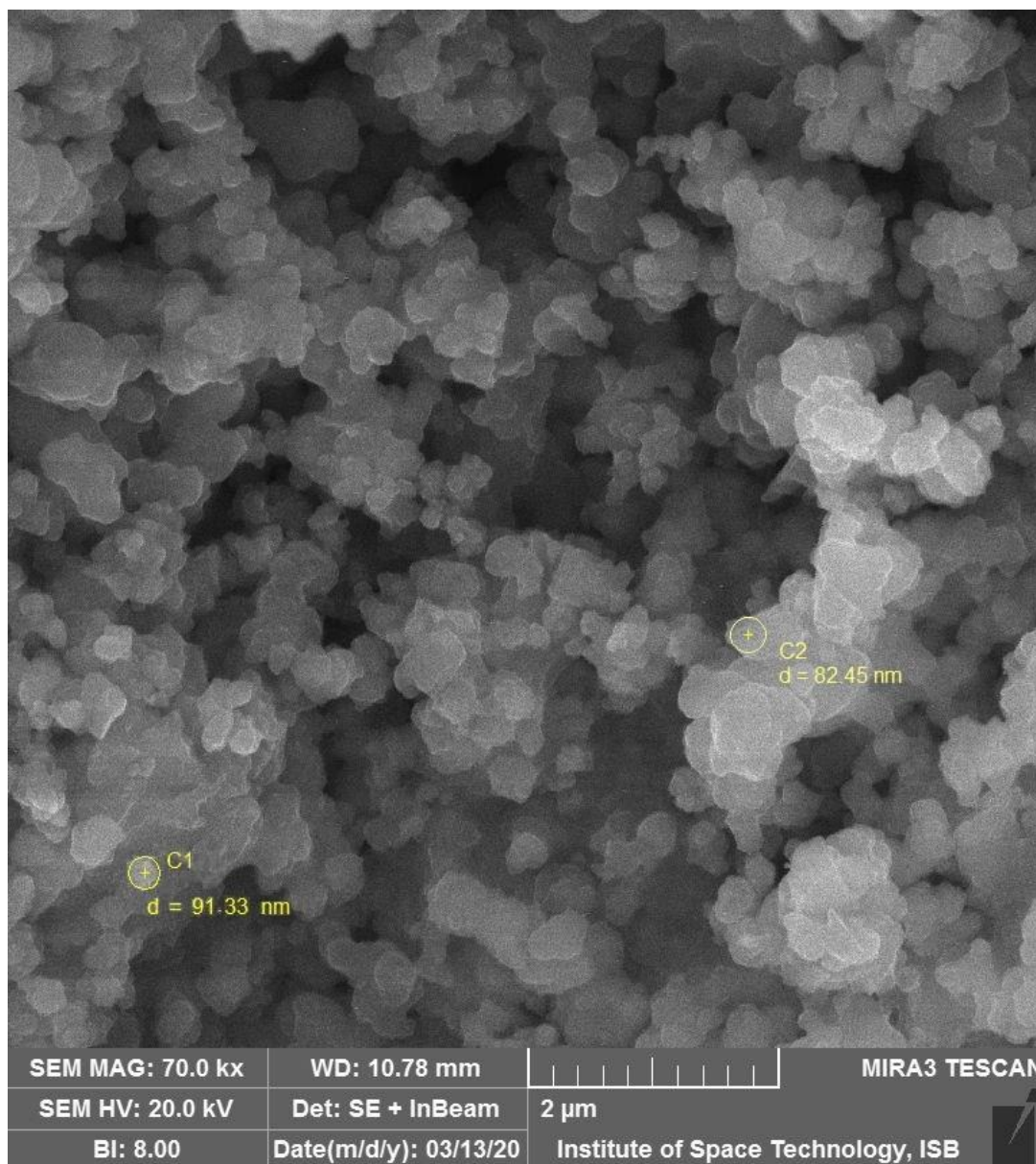


Figure 6.5: FESEM analysis of Nickle Sulphide

6.3 Electron dispersive spectroscopy (EDX):

Electron Dispersive Spectroscopy analysis of Nickel cobalt sulphide was carried out by the detector attached to the inside of the Field Emission Scanning Electron Microscope. Electron Dispersive Spectroscopy analysis provides us with the elemental composition of nickle cobalt sulphide. It affirmed the desired amount of nickel, cobalt, and oxygen presence in nickle cobalt sulphide. Ni, Co, and sulphur are 20.73, 33.51 and

45.76 by atomic weight percentage, respectively. It shows that cobalt cations were replaced by nickel cations which affirmed the faster ion transport mechanism and decrease the resistivity problem. From Electron Dispersive Spectroscopy measurement NiCo_2S_4 . Electron Dispersive Spectroscopy spectrum shows sharp peaks of Cobalt and sulphur in figure shown below:

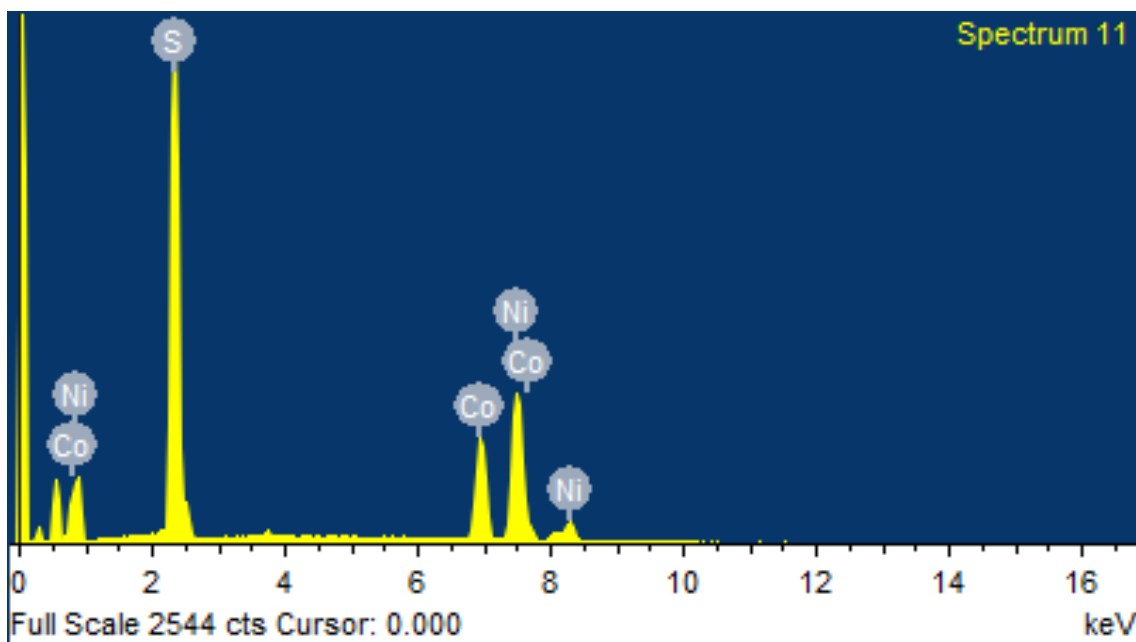


Figure 6.6: EDS spectrum of NCS

And below is a table that shows the EDS of the elements analyzed:

Table 6.1: EDS of elements analyzed of ZNCS sample

Element	Weight percentage	Atomic percentage
Nickle	26.24	20.73
Cobalt	42.25	33.51
Sulphur	31.51	45.76

Elemental analysis of zinc nickel cobalt sulphide was performed by the Electron Dispersive Spectroscopy detector attached to the Field Emission Scanning Electron Microscope. Electron Dispersive Spectroscopy analysis confirmed the desired elements

Zinc, Nickel, Cobalt, and Sulphur of 15.33, 15.51, 17.82 and 51.35 atomic weight percent, respectively. Electron Dispersive Spectroscopy analysis affirmed that Cobalt cations were replaced by zinc and nickel cations which limits the high resistivity problem of the cobalt oxide as the ions transport mechanism was enhanced by the replacement of cations. Cobalt and oxygen give sharp peaks in EDS whereas zinc and nickel give less intense peaks. From Electron Dispersive Spectroscopy measurements $Zn_{0.94}Ni_{0.96}Co_{1.1}S_4$. Electron Dispersive Spectroscopy spectrum in Figure shown below:

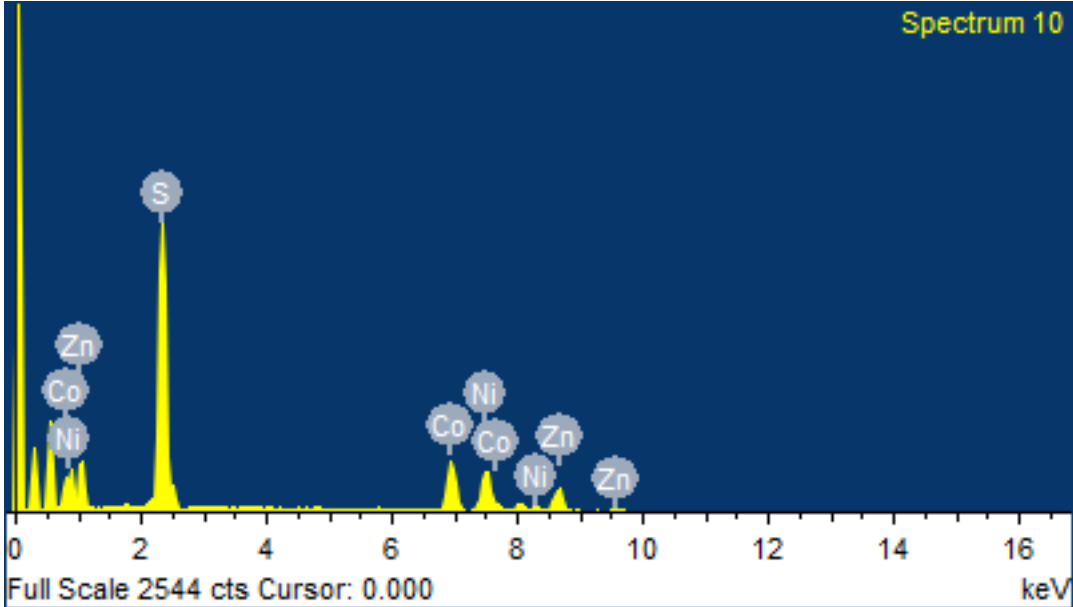


Figure 6.7: EDS spectrum of ZNCS

And below is a table that shows the EDS of the elements analyzed:

Table 6.2: EDS of elements analyzed of NCS sample

Element	Weight percentage	Atomic percentage
Nickle	19.76	15.51
Cobalt	22.78	17.82
Zinc	21.74	15.33
Sulphur	35.72	51.35

Electron Dispersive Spectroscopy analysis of nickel sulphide was carried out by the detector attached to the inside of the Field Emission Scanning Electron Microscope. Electron Dispersive Spectroscopy analysis provides us with the elemental composition of nickel sulphide. It affirmed the desired amount of nickel and sulphur presence in nickel sulphide. Nickel and sulphur are 47.76 and 52.24 by atomic weight percentage, respectively. The electrochemical tests affirmed the faster ion transport mechanism and a decrease in the resistivity problem. Electron Dispersive Spectroscopy spectrum shows sharp peaks of Cobalt and sulphur in figure shown below:

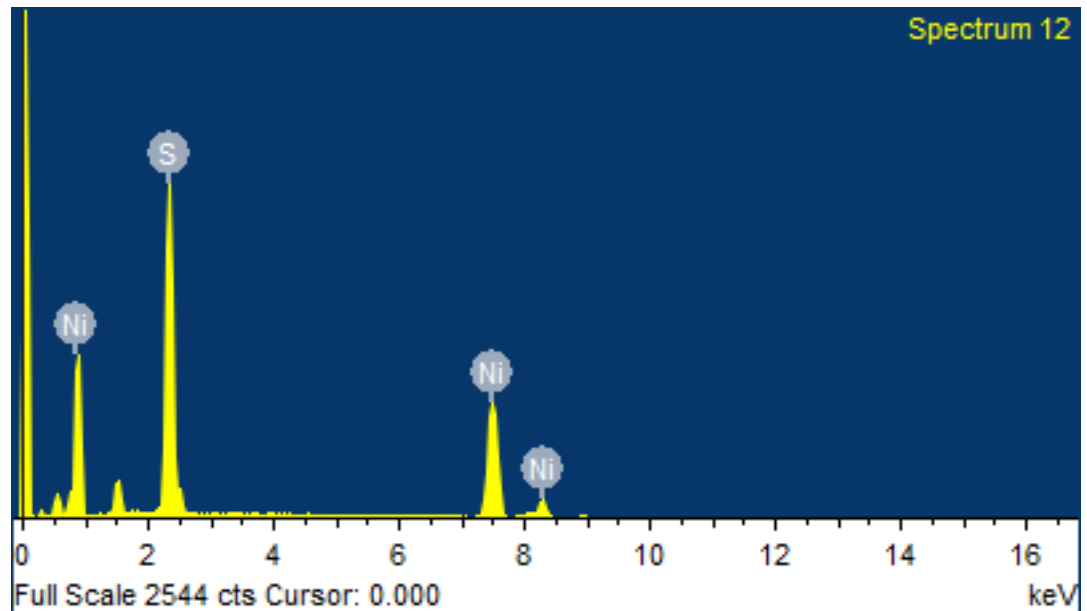


Figure 6.8: EDS spectrum of NS

And below is a table that shows the EDS of the elements analyzed:

Table 6.3: EDS of elements analyzed of NS sample

Element	Weight percentage	Atomic percentage
Nickle	62.60	47.76
Sulphur	37.40	52.24

6.6 Cyclic Voltammetry (CV):

Cyclic Voltammetry has been performed, in an attempt for the check of faradaic response of NS, NCS, ZNCS respectively at a different scan rate of 10 mV s^{-1} , 20 mVs^{-1} , 50 mVs^{-1} and 100 mVs^{-1} with a potential window of -0.1 V to 0.5 V . The non-rectangular shape as shown in the following figures confirms the faradaic redox reaction and the pseudocapacitive nature of NS, NCS and ZNCS electrode material. We observed CV curves for ZNCS as well as in NS and NCS; and redox peaks were observed. The peak position of samples was at different ranges which represents the unconventional materials having different polarization. Increasing the scan rate peaks were shifted from its position shows the different polarization and redox reaction is limited results in less prominent peaks. Ternary sulphide nanoparticles ZNCS evinces the highest specific capacitance as compared to nickle sulphide and nickle cobalt sulphide. ZNCS has greater integrated area as compared to the NS, NCS and ZNCS due to the replacement of Cobalt cations with the Zinc and Nickel cations which results in the better electrochemical performance as well as the specific capacitance. Specific capacitance decrease with increasing scan rate due to limited faradaic redox reaction as less active sites available as compared to the lowest scan rate at which highest capacitance due to the active redox sites abundance. The specific capacitance of ZNCS, NCS, and NS was calculated at different scan rates from employing following formula:

$$C_s = \frac{\int idV}{(V_s \times m \times \Delta V)}$$

Here C_s represents specific capacitance, $\int idV$ is the integrated scan area, V_s represents scan rate, m is the active mass which was 0.01 mg and ΔV is the operating potential window.

Zinc nickle cobalt sulphide (ZNCS) nanoparticles exhibits capacitance of 2113.1735 Fg^{-1} , 1645.78 Fg^{-1} , 1371.899 Fg^{-1} and 1028.26 Fg^{-1} . Whereas NS and NCS shows 271.3909 Fg^{-1} , 231.8650 Fg^{-1} , 186.644 Fg^{-1} , 113.55 Fg^{-1} and 1050.7988 Fg^{-1} , 725.145 Fg^{-1} , 534.6458 Fg^{-1} and 430.9452 Fg^{-1} at 10 mVs^{-1} , 20 mVs^{-1} , 50 mVs^{-1} , 100 mVs^{-1} respectively because integrated area of Nickle Sulphide (NS) and Nickle cobalt sulphide (NCS) was smaller in comparison with Zinc Nickle Cobalt Sulphide (ZNCS).

6.6.1 Nickle Sulphide:

Figure 6.9 exhibits the Cyclic Voltammetry (CV) curves for nickle sulphide at the scan rate of 10 mVs^{-1} , 20 mVs^{-1} , 50 mVs^{-1} and 100 mVs^{-1} . The CV was performed at the potential range of -0.1 V to 0.5 V. The active material was deposited onto a glassy carbon electrode. As it is conspicuously visible from the CV curves, the peak current increases with an increase in the scan rate over the active material. Thus, the shape of the CV curves for Nickle Sulphide evinces the pseudocapacitive property of Nickle Sulphide (NS). The value of current in response to the applied potential difference increase with the scan rate.

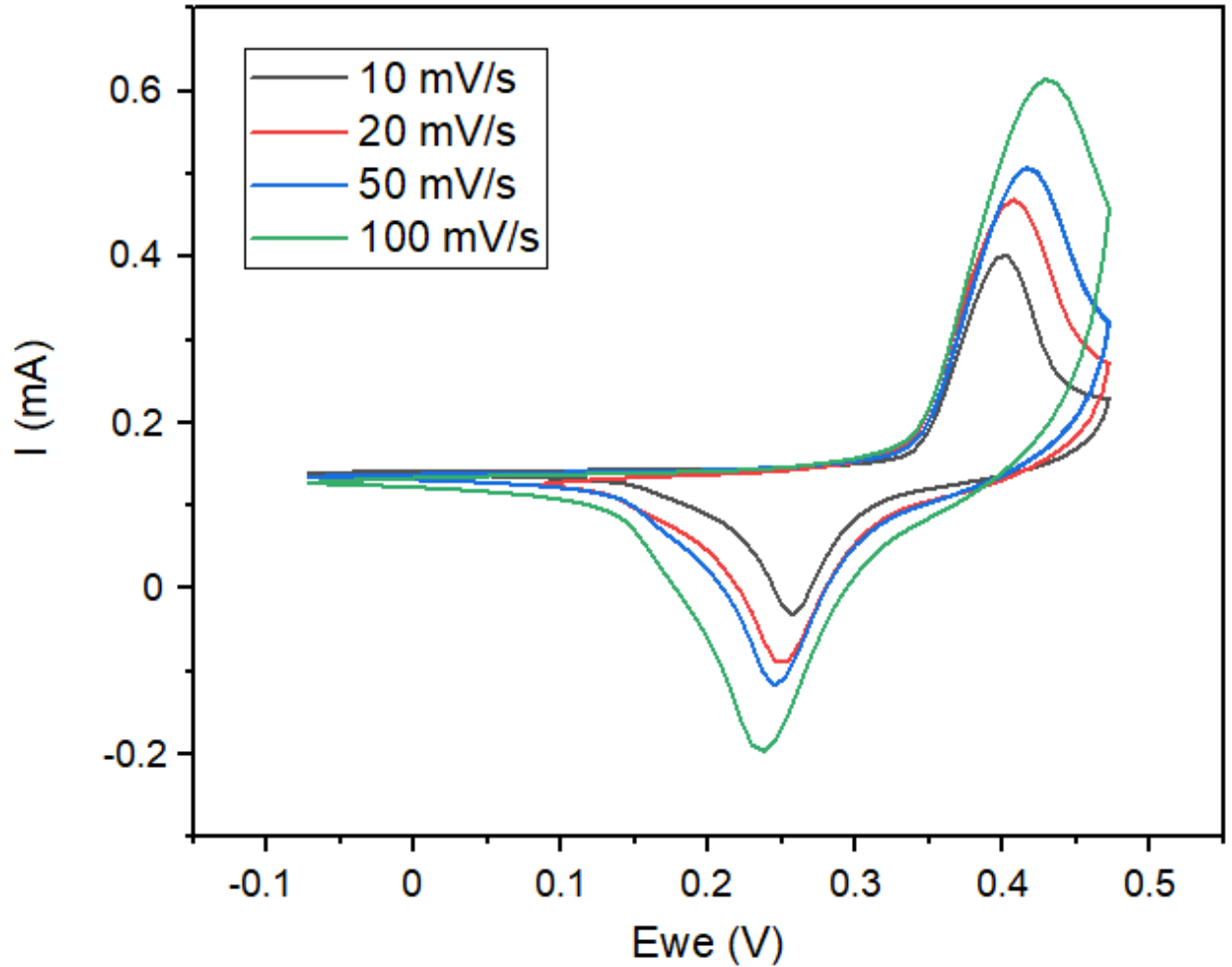


Figure 6.9: CV of Nickle Sulphide (NS)

6.6.2 Nickle Cobalt Sulphide:

Figure 6.10 exhibits the Cyclic Voltammetry (CV) curves for nickle sulphide at the scan rate of 10 mVs^{-1} , 20 mVs^{-1} , 50 mVs^{-1} and 100 mVs^{-1} . The CV was performed at the potential range of -0.1 V to 0.5 V . The active material was deposited onto a glassy carbon electrode. As it is conspicuously visible from the CV curves, the peak current increases with an increase in the scan rate over the active material. Thus, the shape of the CV curves for Nickle Cobalt Sulphide evinces the pseudocapacitive property of Nickle Cobalt Sulphide (NS). The value of current as a result of the applied potential difference increase with the scan rate.

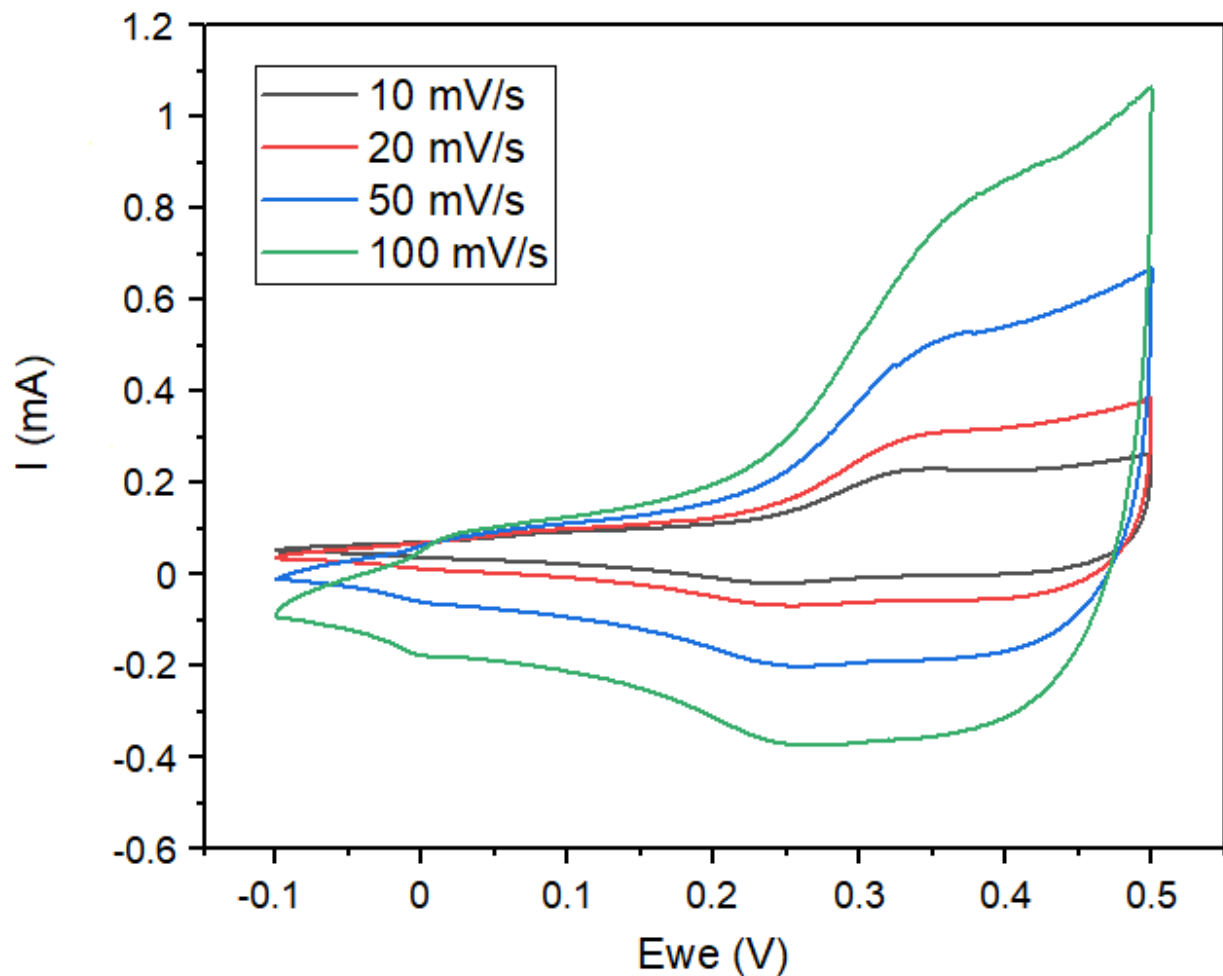


Figure 6.10: CV of Nickle Cobalt Sulphide (NCS)

6.6.3 Zinc Nickle Cobalt Sulphide:

Figure 6.11 exhibits the Cyclic Voltammetry (CV) curves for nickle sulphide at the scan rate of 10 mVs^{-1} , 20 mVs^{-1} , 50 mVs^{-1} and 100 mVs^{-1} . The CV was performed at the potential range of -0.1 V to 0.5 V . The active material was deposited onto a glassy carbon electrode. As it is conspicuously visible from the CV curves, the peak current increases with an increase in the scan rate over the active material. Thus, the shape of the CV curves for Zinc Nickle Cobalt Sulphide evinces the pseudocapacitive property of Zinc Nickle Cobalt Sulphide (ZNCS). The value of current in response to the applied potential difference increase with the scan rate.

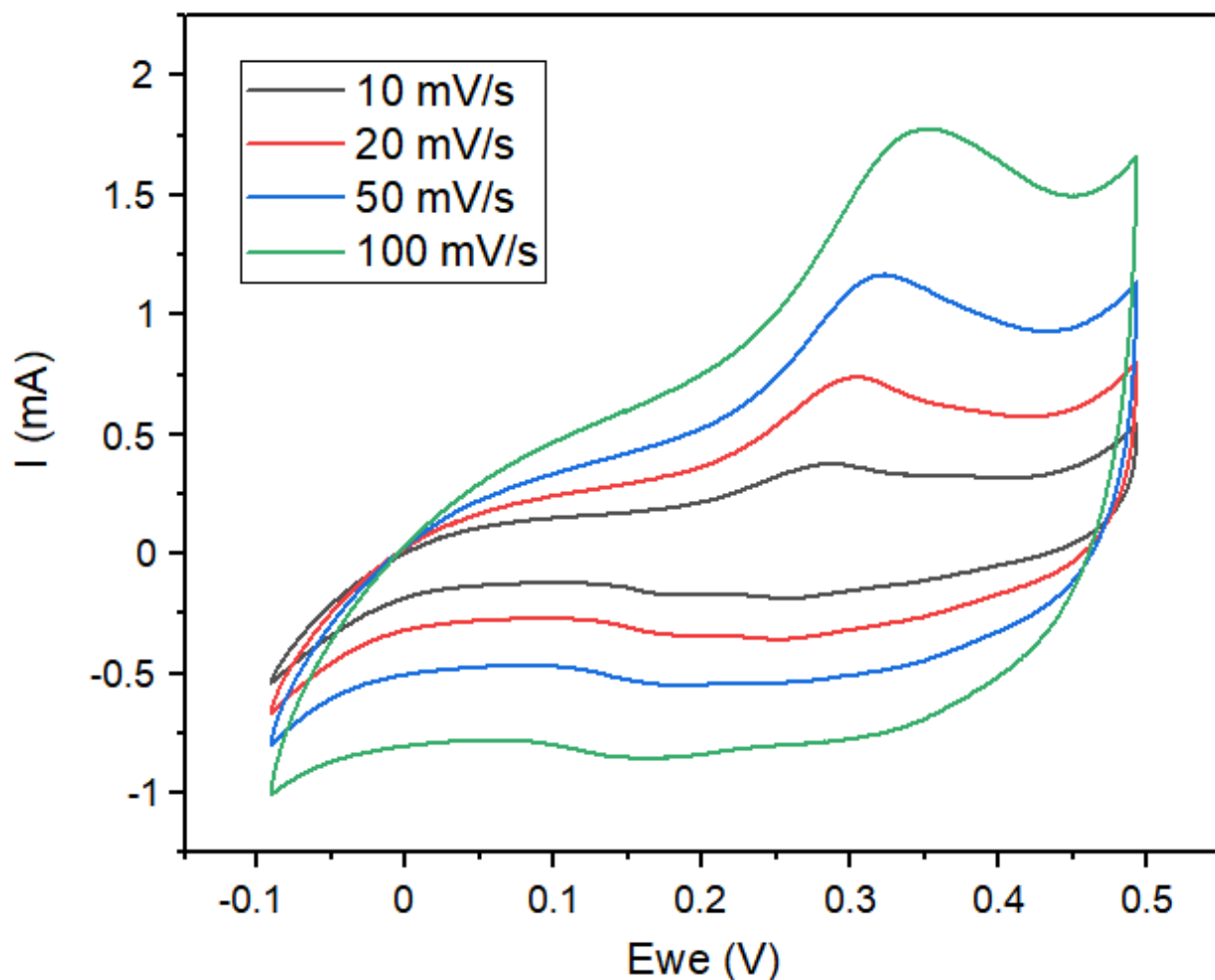


Figure 6.11: CV of Zinc Nickle Cobalt Sulphide (ZNCS)

6.7 Galvanostatic charge-discharge (GCD):

6.7.1 Nickle Sulphide:

Galvanostatic charge discharge (GCD) was performed to study more capacitive properties of Nickle Sulphide after learning the capacitive nature of NS through Cyclic Voltammetry curve. GCD at different current densities was performed in order to study the abilities of NS to sustain charge in detail as shown in fig. 6.14, the maximum time for charge sustaining was seen on the current density of 5 Ag^{-1} . As we increased the current density the charge sustain time declined which was in result of low capacitance. Calculated capacitance for Nickle Sulphide (NS) was 271.3909 Fg^{-1} , 231.8650 Fg^{-1} , 186.644 Fg^{-1} , 113.55 Fg^{-1} .

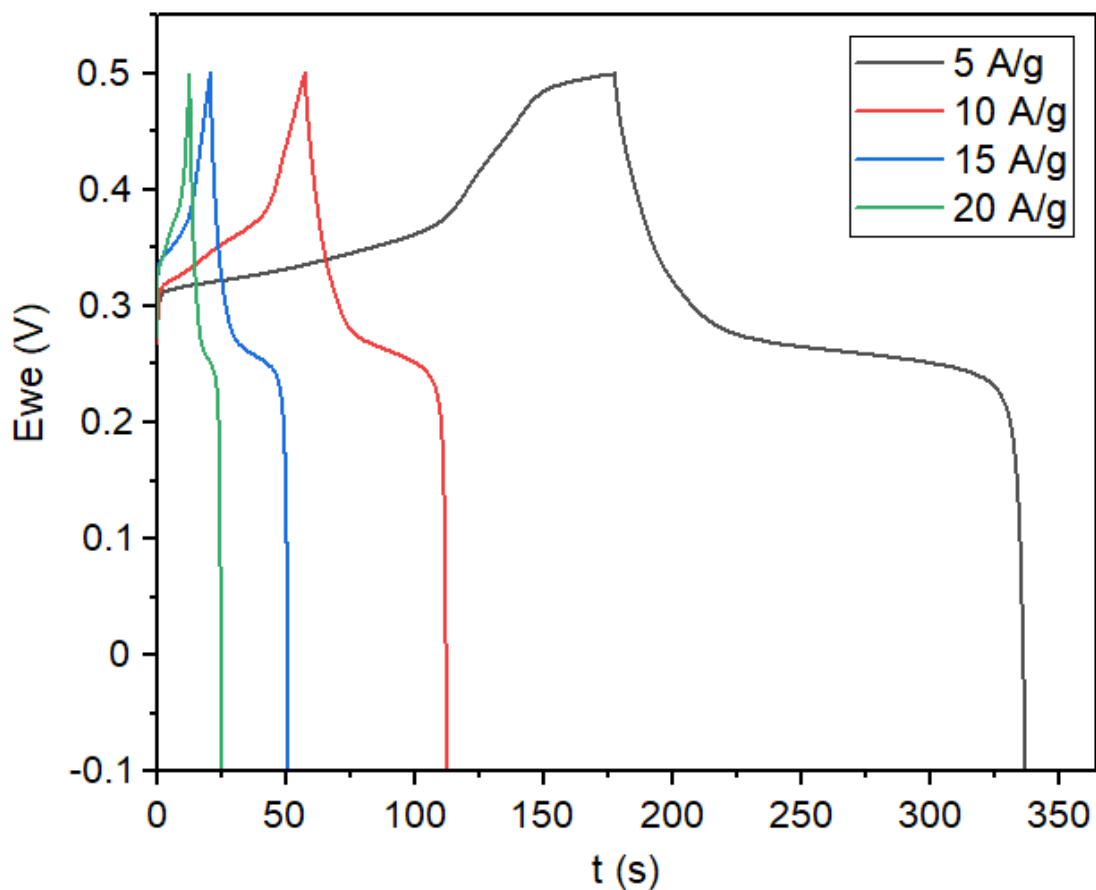


Figure 6.12: GCD of Nickle Sulphide (NS)

6.7.2 Nickle Cobalt Sulphide:

GCD was performed to study more capacitive properties of Nickle Cobalt Sulphide after learning the capacitive nature of NCS through Cyclic Voltammetry curve. GCD at different current densities was performed in order to study the abilities of NCS to sustain charge in detail as shown in fig. 6.13, the maximum time for charge sustaining was seen on the current density of 5 Ag^{-1} . As we increased the current density the charge sustain time declined which was in result of low capacitance. Calculated Capacitance for NCS was $1050.7988 \text{ Fg}^{-1}$, 725.145 Fg^{-1} , 534.6458 Fg^{-1} and 430.9452 Fg^{-1} .

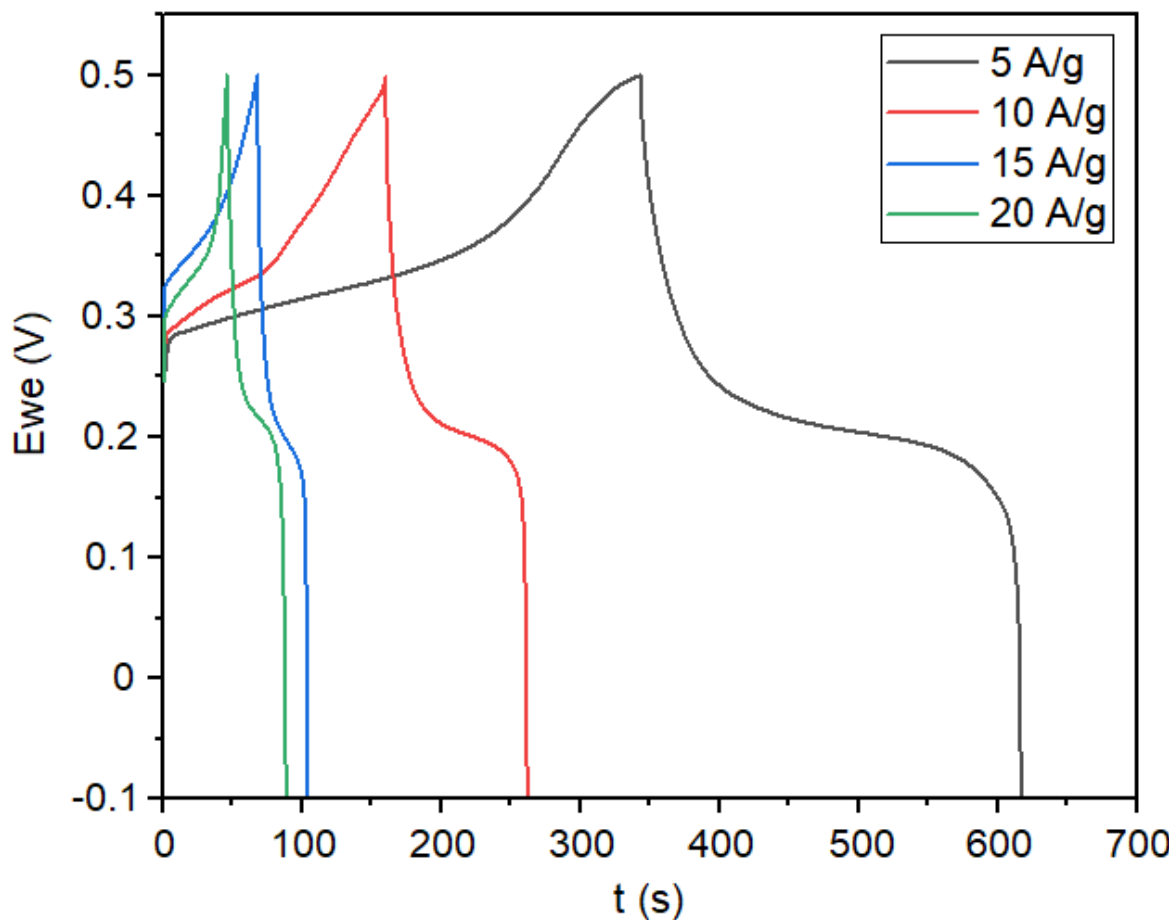


Figure 6.13: GCD of Nickle Cobalt Sulphide (NCS)

6.7.3 Zinc Nickle Cobalt Sulphide:

GCD was performed to study more capacitive properties of Nickel Cobalt Sulphide after learning the capacitive nature of NCS through Cyclic Voltammetry curve. GCD at different current densities was performed in order to study the abilities of ZNCS to sustain charge in detail as shown in fig. 6.14, the maximum time for charge sustaining was seen on the current density of 5 Ag^{-1} . As we increased the current density the charge sustain time declined which was in result of low capacitance. Calculated Capacitance for ZNCS was $2113.1735 \text{ Fg}^{-1}$, 1645.78 Fg^{-1} , 1371.899 Fg^{-1} and 1028.26 Fg^{-1} .

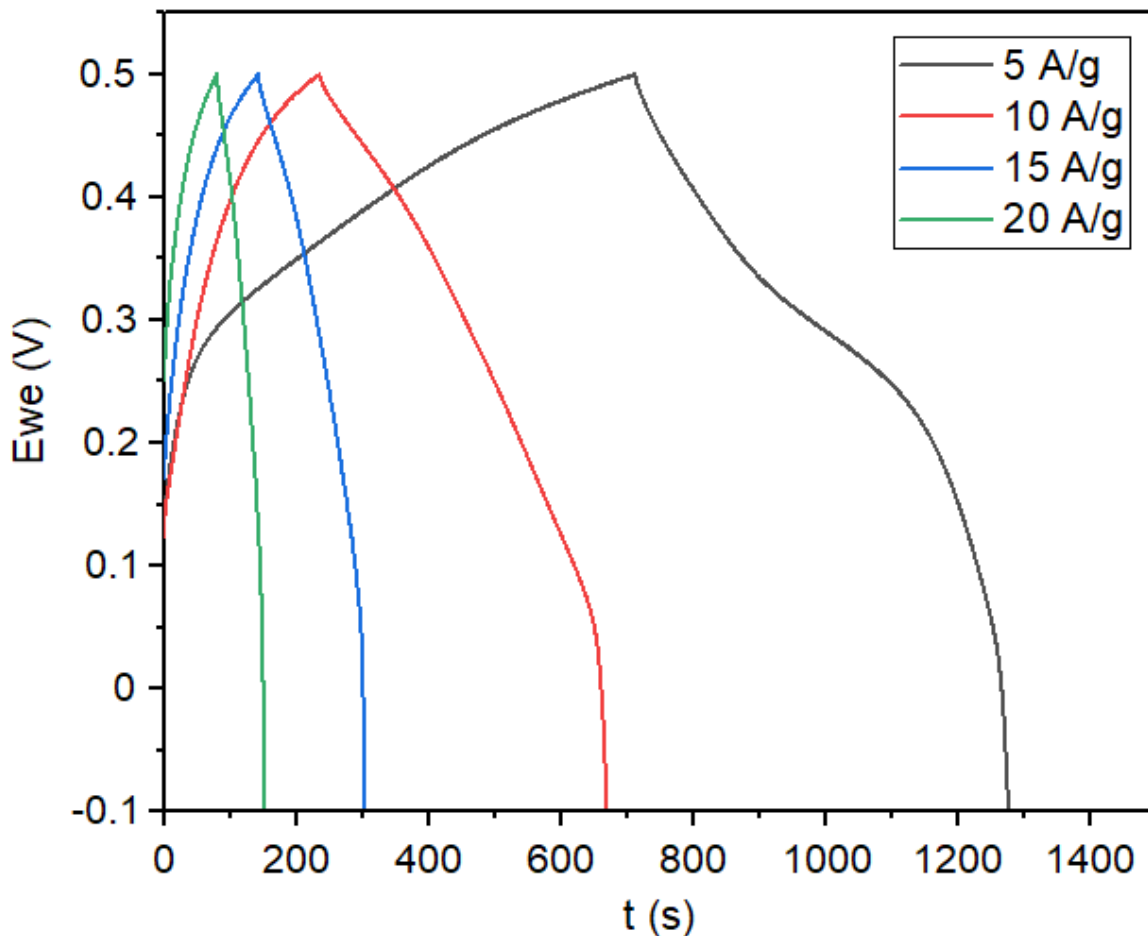


Figure 6.14: GCD of Zinc Nickle Cobalt Sulphide (ZNCS)

6.8 Cyclic stability:

Cyclic performance of prepared electrode material was also analyzed through CV and GCD cycles. ZNCS shows excellent cyclic response and columbic efficiency. Columbic Efficiency was 99.9% and 99.4% capacitance retention after 1000 cycles of the CV which shows the excellent cyclic stability of Zinc Nickle Cobalt Sulphide (ZNCS). ZNCS also evinces good cyclic response in charge-discharge about 99.4% capacitance retention after 1000 cycles at 50 A g⁻¹.

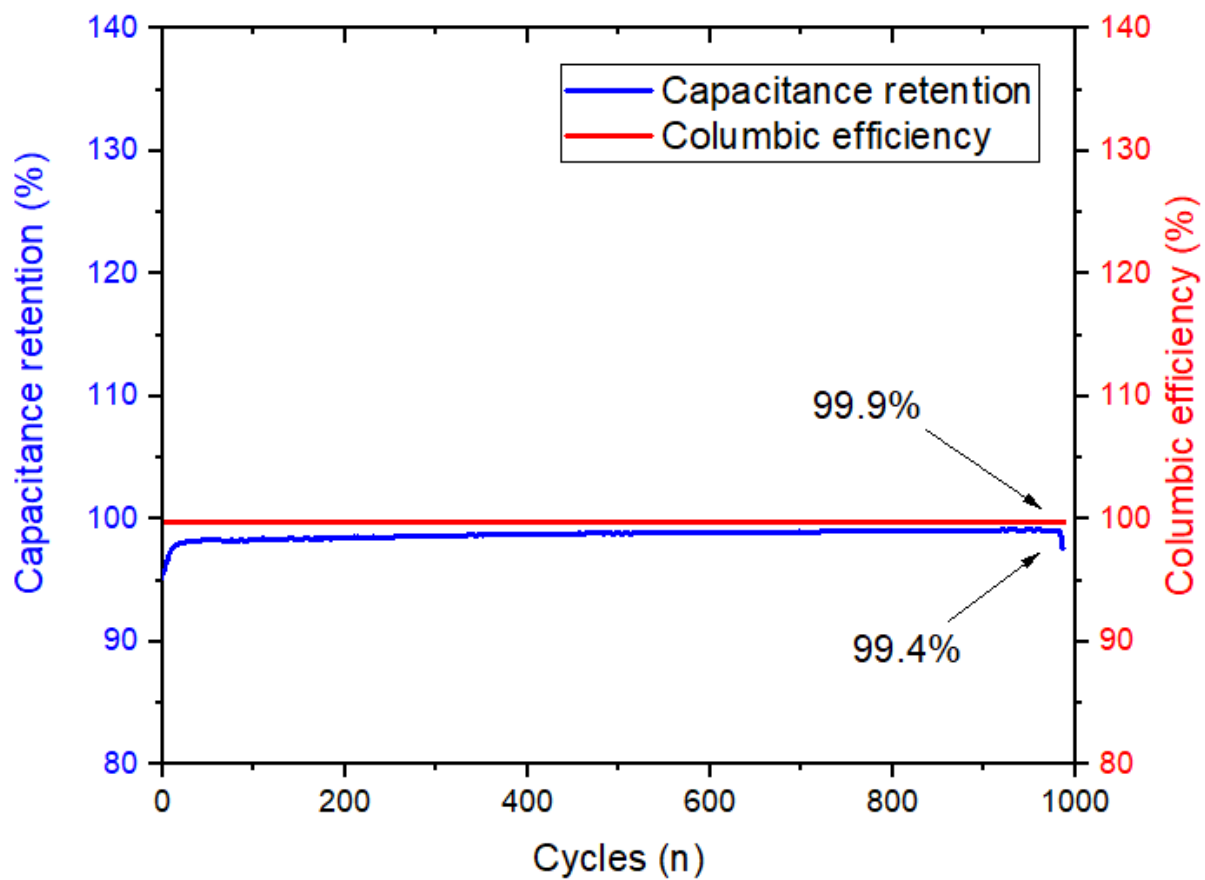


Figure 6.14: Cyclic stability of Zinc Nickel Cobalt Sulphide (ZNCS)

Conclusion

Ternary sulphide nanoparticles based on Zn, Ni and Co were successfully synthesized through the hydrothermal route. XRD and EDX was performed to study crystal structure, SEM was performed to carry out the study of microstructural properties. Electrochemical characterization was studied by VSP biologic work station. High specific capacitance and energy density were achieved by this synthesized material due to its higher surface area, nanoparticle morphology, and synergistic contributions of the individual components. ZNCS exhibited a higher capacitance of 2113 Fg^{-1} ; which was significantly higher than binary and single sulfides (Nickel Cobalt Sulphide and Nickel Sulphide) synthesized through the same route. In addition, the material demonstrated good long term cyclic stability. Calculated Capacitance for ZNCS was 2113.173 Fg^{-1} , 1645.78 Fg^{-1} , 1371.899 Fg^{-1} and 1028.26 Fg^{-1} at the current densities of 5, 10, 15 and 20 A/g respectively. ZNCS nanoparticles exhibited excellent capacitance retention of 99.4% with a coulombic efficiency of 99.9 % after 1000 cycles at 50 A g^{-1} . This performance evinces that this material will meet the modern-day energy applications demands.

REFERENCES:

- [1] C. De Fraiture, M. Giordano, and Y. Liao, "Biofuels and implications for agricultural water use : blue impacts of green energy," vol. 1, pp. 67–81, (2008).
- [2] K. Zhu, Y. Sun, R. Wang, Z. Shan, and K. Liu, "Fast synthesis of uniform mesoporous titania submicrospheres with high tap densities for high-volumetric performance Li-ion batteries," no. February, pp. 1–3, (2017).
- [3] A. Yu, V. Chabot, J. Zhang, *Electrochemical supercapacitors for energy storage and delivery: fundamentals and applications*, CRC press, (2013).
- [4] J.P. Barton, D.G. Infield, *IEEE transactions on energy conversion*, 19 (2004) 441-448.
- [5] S. Cavaliere, S. Subianto, I. Savych, D.J. Jones, J. Rozière, *Energy & Environmental Science*, 4 (2011) 4761-4785.
- [6] W. Li, J. Liu, D. Zhao, *Nature Reviews Materials*, 1 (2016) 16023.
- [7] J.W. Lee, A.S. Hall, J.-D. Kim, T.E. Mallouk, *Chemistry of Materials*, 24 (2012) 1158-1164.
- [8] B. Conway, *Introduction and Historical Perspective, Electrochemical Supercapacitors*, Springer, (1999), pp. 1-9.
- [9] L. Zhang, X. Hu, Z. Wang, F. Sun, D.G. Dorrell, *Renewable and Sustainable Energy Reviews*, 81 (2018) 1868-1878.
- [10] A. Muzaffar, M.B. Ahamed, K. Deshmukh, J. Thirumalai, *Renewable and Sustainable Energy Reviews*, 101 (2019) 123-145.
- [11] S. Palchoudhury, K. Ramasamy, R.K. Gupta, A. Gupta, *Frontiers in Materials*, 5 (2019) 83.
- [12] L. Halder, A. Maitra, A.K. Das, R. Bera, S.K. Karan, S. Paria, A. Bera, S.K. Si, B.B. Khatua, *ACS Applied Electronic Materials*, 1 (2019) 189-197.
- [13] M. Tebyetekerwa, I. Marriam, Z. Xu, S. Yang, H. Zhang, F. Zabihi, R. Jose, S. Peng, M. Zhu, S. Ramakrishna, *Energy & Environmental Science*, (2019).
- [14] G. Li, Z. Li, P. Zhang, H. Zhang, Y. Wu, *Pure and Applied Chemistry*, 80 (2008) 2553-2563.
- [15] N. Syarif, T. Ivandini, W. Wibowoa, *Int. Trans. J. Eng. Manage., Appl. Sci Technol*, 3 (2012) 21-34.76
- [16] Q. Cheng, J. Tang, J. Ma, H. Zhang, N. Shinya, L.-C. Qin, *Physical Chemistry Chemical Physics*, 13 (2011) 17615-17624.
- [17] C. Du, N. Pan, *Nanotech. L. & Bus.*, 4 (2007) 3.
- [18] K.S. Novoselov, A.K. Geim, S.V. Morozov, D. Jiang, Y. Zhang, S.V. Dubonos, I.V. Grigorieva, A.A. Firsov, *science*, 306 (2004) 666-669.
- [19] Y. Zhu, S. Murali, M.D. Stoller, K. Ganesh, W. Cai, P.J. Ferreira, A. Pirkle, R.M. Wallace, K.A. Cychoz, M. Thommes, *science*, 332 (2011) 1537-1541.

- [20] S. Bhadra, D. Khastgir, N.K. Singha, J.H. Lee, *Progress in polymer science*, 34 (2009) 783-810.
- [21] S.-C. Huang, S.-M. Huang, H. Ng, R. Kaner, *Synthetic metals*, 57 (1993) 4047-4052.
- [22] A. Rudge, I. Raistrick, S. Gottesfeld, J.P. Ferraris, *Electrochimica Acta*, 39 (1994) 273-287.
- [23] L. Ren, G. Zhang, Z. Yan, L. Kang, H. Xu, F. Shi, Z. Lei, Z.-H. Liu, *ACS applied materials & interfaces*, 7 (2015) 28294-28302.
- [24] C.-C. Hu, C.-H. Chu, *Materials chemistry and physics*, 65 (2000) 329-338.
- [25] H. Karami, M.F. Mousavi, M. Shamsipur, *Journal of Power Sources*, 117 (2003) 255-259.
- [26] A. Eftekhari, P. Jafarkhani, *Polymer journal*, 38 (2006) 651.
- [27] J.F. Mike, J.L. Lutkenhaus, *Journal of Polymer Science Part B: Polymer Physics*, 51 (2013) 468-480.
- [28] Y. Li, X. Zhao, Q. Xu, Q. Zhang, D. Chen, *Langmuir*, 27 (2011) 6458-6463.
- [29] H. Guan, L.-Z. Fan, H. Zhang, X. Qu, *Electrochimica Acta*, 56 (2010) 964-968.
- [30] D. Vonlanthen, P. Lazarev, K.A. See, F. Wudl, A.J. Heeger, *Advanced Materials*, 26 (2014) 5095-5100.
- [31] X. Li, C. Zhang, S. Xin, Z. Yang, Y. Li, D. Zhang, P. Yao, *ACS applied materials & interfaces*, 8 (2016) 21373-21380.
- [32] J.S. Choi, C.H. Yo, *Inorganic Chemistry*, 13 (1974) 1720-1724.
- [33] T.-C. Liu, W. Pell, B. Conway, *Electrochimica Acta*, 44 (1999) 2829-2842.
- [34] H.-J. Qiu, L. Liu, Y.-P. Mu, H.-J. Zhang, Y. Wang, *Nano Research*, 8 (2015) 321-339.
- [35] J. Mei, Y. Zhang, T. Liao, Z. Sun, S.X. Dou, *National Science Review*, 5 (2017) 389-416.
- [36] C. Yuan, L. Yang, L. Hou, L. Shen, X. Zhang, X.W.D. Lou, *Energy & Environmental Science*, 5 (2012) 7883-7887.
- [37] Q. Wang, B. Liu, X. Wang, S. Ran, L. Wang, D. Chen, G. Shen, *Journal of Materials Chemistry*, 22 (2012) 21647-21653.
- [38] S.-K. Chang, K.-T. Lee, Z. Zainal, K.-B. Tan, N.A. Yusof, W.M.D.W. Yusoff, J.-F. Lee, N.-L. Wu, *Electrochimica Acta*, 67 (2012) 67-72.
- [39] C. Yuan, J. Li, L. Hou, L. Yang, L. Shen, X. Zhang, *Journal of Materials Chemistry*, 22 (2012) 16084-16090.
- [40] G. Zhang, T. Wang, X. Yu, H. Zhang, H. Duan, B. Lu, *Nano Energy*, 2 (2013) 586-594.
- [41] T. Huang, C. Zhao, R. Zheng, Y. Zhang, Z. Hu, *Ionics*, 21 (2015) 3109-3115.
- [42] H.H. Jaffé, M. Orchin, (1962).
- [43] H.H. Willard, L.L. Merritt Jr, J.A. Dean, F.A. Settle Jr, (1988).
- [44] T. Owen, Agilent Technologie, German, (2000).

- [45] J.W. Robinson, E.M.S. Frame, G.M. Frame II, Undergraduate instrumental analysis, CRC press, (2014).
- [46] D.A. Skoog, D.M. West, F.J. Holler, S. Crouch, Fundamentals of analytical chemistry, Nelson Education, (2013).
- [47] H.-H. Perkampus, UV-VIS Spectroscopy and its Applications, Springer Science & Business Media, (2013).
- [48] B. Warren, there is no corresponding record for this reference.
- [49] J.I. Goldstein, D.E. Newbury, J.R. Michael, N.W. Ritchie, J.H.J. Scott, D.C. Joy, Scanning electron microscopy and X-ray microanalysis, Springer, (2017).
- [50] J.F. Watts, J. Wolstenholme, An Introduction to Surface Analysis by XPS and AES, by John F. Watts, John Wolstenholme, pp. 224. ISBN 0-470-84713-1. Wiley-VCH, May 2003., (2003) 224.
- [51] S. Pennycook, L. Boatner, Nature, 336 (1988) 565.
- [52] J.B. Condon, Surface area and porosity determinations by physisorption: measurements and theory, Elsevier, (2006).
- [53] H.M. Rootare, C.F. Prenzlów, The Journal of physical chemistry, 71 (1967) 2733-2736.
- [54] B.K. Kim, S. Sy, A. Yu, J. Zhang, Handbook of Clean Energy Systems, (2015) 1-2578
- [55] N.K. Bakirhan, B. Uslu, S.A. Ozkan, The detection of pesticide in foods using electrochemical sensors, Food Safety and Preservation, Elsevier, (2018), pp. 91-141.
- [56] F. Rohrbach, H. Karadeniz, A. Erdem, M. Famulok, G. Mayer, Analytical biochemistry, 421 (2012) 454-459.
- [57] D.T. Tran, V. Vermeeren, L. Grieten, S. Wenmackers, P. Wagner, J. Pollet, K.P. Janssen, L. Michiels, J. Lammertyn, Biosensors and Bioelectronics, 26 (2011) 2987
- [58] A.-E. Radi, J.L. Acero Sánchez, E. Baldrich, C.K. O'Sullivan, Analytical chemistry, 77 (2005) 6320-6323.
- [59] A. Bogomolova, E. Komarova, K. Reber, T. Gerasimov, O. Yavuz, S. Bhatt, M. Aldissi, Analytical Chemistry, 81 (2009) 3944-3949.
- [60] N. Reichbach, M. Mellincovsky, M. Peretz, A. Kuperman, IEEE Transactions on Energy Conversion, 31 (2016) 404-406.
- [61] W. Li, J. Liu, D. Zhao, Nature Reviews Materials, 1 (2016) 16023.
- [62] J.W. Lee, A.S. Hall, J.-D. Kim, T.E. Mallouk, Chemistry of Materials, 24 (2012) 1158-1164.
- [63] B. Conway, Introduction and Historical Perspective, Electrochemical Supercapacitors, Springer, (1999), pp. 1-9.
- [64] L. Zhang, X. Hu, Z. Wang, F. Sun, D.G. Dorrell, Renewable and Sustainable Energy Reviews, 81 (2018) 1868-1878.
- [65] A. Muzaffar, M.B. Ahamed, K. Deshmukh, J. Thirumalai, Renewable and Sustainable Energy Reviews, 101 (2019) 123-145.

- [66] H.-H. Perkampus, *UV-VIS Spectroscopy and its Applications*, Springer Science & Business Media, (2013).
- [67] B. Warren, there is no corresponding record for this reference.
- [68] J.I. Goldstein, D.E. Newbury, J.R. Michael, N.W. Ritchie, J.H.J. Scott, D.C. Joy, *Scanning electron microscopy and X-ray microanalysis*, Springer, (2017).
- [69] J.F. Watts, J. Wolstenholme, *An Introduction to Surface Analysis by XPS and AES*, by John F. Watts, John Wolstenholme, pp. 224. ISBN 0-470-84713-1. Wiley-VCH, May 2003., (2003) 224.
- [70] S. Pennycook, L. Boatner, *Nature*, 336 (1988) 565.
- [71] J.B. Condon, *Surface area and porosity determinations by physisorption: measurements and theory*, Elsevier, (2006).
- [72] H.M. Rootare, C.F. Prenzlow, *The Journal of physical chemistry*, 71 (1967) 2733-2736.
- [73] B.K. Kim, S. Sy, A. Yu, J. Zhang, *Handbook of Clean Energy Systems*, (2015) 1-2578
- [74] N.K. Bakirhan, B. Uslu, S.A. Ozkan, *The detection of pesticide in foods using electrochemical sensors*, *Food Safety and Preservation*, Elsevier, (2018), pp. 91-141.
- [75] F. Rohrbach, H. Karadeniz, A. Erdem, M. Famulok, G. Mayer, *Analytical biochemistry*, 421 (2012) 454-459.
- [76] J.W. Robinson, E.M.S. Frame, G.M. Frame II, *Undergraduate instrumental analysis*, CRC press, (2014).
- [77] D.A. Skoog, D.M. West, F.J. Holler, S. Crouch, *Fundamentals of analytical chemistry*, Nelson Education, (2013).